

ELECTROMAGNETIC DECAY OF THE
1.7- AND 2.43-MeV LEVELS IN ${}^9\text{Be}$

Thesis by

Paul Walton Purdom, Jr.

In Partial Fulfillment of the Requirements

For the Degree of
Doctor of Philosophy

California Institute of Technology

Pasadena, California

1966

(Submitted January 1966)

ACKNOWLEDGMENTS

I wish to thank Dr. P. A. Seeger and Dr. R. W. Kavanagh for their great help in the conception, design and execution of the experiment. I wish to thank Mr. C. D. Zaidins for his assistance with the charge state measurements and Dr. F. C. Barker for helping in the calculation of the width of the 2.43-MeV level in ^9Be . I am also indebted to the entire staff of the Kellogg Radiation Laboratory for creating an atmosphere in which the work could be carried out.

ABSTRACT

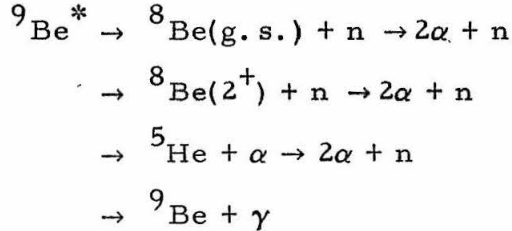
The 1.7- and 2.43-MeV levels in ${}^9\text{Be}$ were populated with the reaction ${}^{11}\text{B}(d, \alpha){}^9\text{Be}^*$ by bombarding thin boron on carbon foils with 1.7-MeV deuterons. The alpha particles were analyzed in energy with a surface-barrier counter set at the unique kinematically determined angle and the recoiling ${}^9\text{Be}$ nuclei at 90° were analyzed in rigidity with a magnetic spectrometer, in energy by a surface-barrier counter at the spectrometer focus, and in velocity by the time delay between an alpha and a ${}^9\text{Be}$ count. When a pulse from the spectrometer counter was in the appropriate delayed coincidence with a pulse from the alpha counter, the two pulses were recorded in a two-dimensional pulse height analyzer. Most of the ${}^9\text{Be}^*$ decay by particle breakup. Only those that gamma decay are detected by the spectrometer counter. Thus the experiment provides a direct measurement of $\Gamma_{\text{rad}}/\Gamma$. Analysis of 384 observed events gives $\Gamma_{\text{rad}}/\Gamma = (1.16 \pm 0.14) \times 10^{-4}$ for the 2.43-MeV level. Combining this ratio with the value of $\Gamma_{\text{rad}} = 0.122 \pm 0.015$ eV found from inelastic electron scattering gives $\Gamma = (1.05 \pm 0.18)$ keV. For the 1.7-MeV level, an upper limit, $\Gamma_{\text{rad}}/\Gamma \leq 2.4 \times 10^{-5}$, was determined.

TABLE OF CONTENTS

	<u>Page</u>
I. Introduction	1
II. Experiment and Apparatus	2
A. Recoil Ion Detection	3
B. Alpha Detection	5
C. Coincidence Detection	6
D. Monitoring Equipment	7
E. Experimental Procedure	7
III. Analysis of Results	11
A. Counting Rate Factor $(N_* - B_*)/N_o$	11
B. Efficiency Factor	13
C. Population Factor α_*/α_o	14
D. Calculation of Γ_{rad}^*/Γ_o	15
IV. Discussion	17
Appendix I	
Boron Foils	19
Appendix II	
Beryllium Charge-State Ratios	24
Appendix III	
Calculation of Particle and Gamma Widths for the 2.43-MeV Level in ^9Be	27
References	33
Tables	35
Figures	50

I. INTRODUCTION

The 2.43-MeV, $J^\pi = 5/2^-$ excited state of ${}^9\text{Be}$ may decay in the following ways:



Decay through the ${}^8\text{Be}$ ground state is greatly inhibited since it requires f-wave neutrons. The 2.43-MeV level of ${}^9\text{Be}$ is below the nominal energies of ${}^8\text{Be}(2^+) + n$ and of ${}^5\text{He} + \alpha$, but since these are broad levels, the decay may proceed at a reduced rate through their low-energy tails. The gamma decay is predominantly M1.

Previous investigators have measured several aspects of the decay. Inelastic proton scattering experiments limit the total width of the 2.43-MeV level to less than 1 keV (Gossett 1955). Inelastic scattering indicates a gamma width of 0.122 ± 0.015 eV (M1) (Edge 1962, Barber 1960) plus 0.0026 ± 0.0001 eV (E2)(Ngoc 1963). Inelastic neutron scattering shows that the level decays by way of ${}^8\text{Be}(\text{g. s.}) + n$ 0.12 ± 0.05 of the time (Marion 1959). So far, no experiment has been able to distinguish between decays through ${}^8\text{Be}(2^+) + n$ and those through ${}^5\text{He} + \alpha$.

Henley (1960) has calculated the partial widths for the various particle decay modes, using the alpha model. His calculations indicate that the total width of the 2.43-MeV level should be about $\frac{1}{4}$ keV and that the primary decay mode should be ${}^9\text{Be}^* \rightarrow {}^5\text{He} + \alpha \rightarrow 2\alpha + n$.

In addition to the $5/2^-$ level at 2.4 MeV, most nuclear models predict a $1/2^-$ level around 2 or 3 MeV (Kunz 1960, Nilsson 1955, Kurath 1956). Such a $1/2^-$ level has not yet been seen in ^9Be .

There have been numerous investigations carried out in attempts to decide whether there is a resonance level near 1.7 MeV, or whether the observed effects can be accounted for in terms of phase space and potential scattering among the particles in the final state. An extensive summary of earlier work in this regard is given by Lucas et al. (Lucas 1964) and need not be repeated here. We consider it here to be a resonance state, with $J^\pi = 1/2^+$, as suggested by comparison of the inelastic electron scattering and photoneutron cross section (Lauritsen 1965). The width of the level observed in the $^{11}\text{B}(d, \alpha)$ reaction is 224 ± 25 keV (Kavanagh 1958), and the gamma width is 4.5 ± 0.6 eV (El) (Ngoc 1963). The decay proceeds primarily via $^8\text{Be}(\text{g. s.}) + n$.

The present work was undertaken to measure the fraction $\Gamma_{\text{rad}}/\Gamma$ of electromagnetic decays of the 2.43-MeV level; an upper limit for the branching ratio of the 1.7-MeV level was also found.

II. EXPERIMENT AND APPARATUS

The number of $^9\text{Be}^*$ recoil ions produced in the reaction $^{11}\text{B}(d, \alpha)^9\text{Be}^*$ was measured by counting the alpha particles from the reaction with energy corresponding to the particular excited state. The recoil $^9\text{Be}^*$ decays after traveling about 10^{-9} cm or less. If the decay occurs by any of the non-electromagnetic modes, the ^9Be recoil is destroyed. The number of electromagnetic decays was measured by counting the number of ^9Be recoils of the proper energy to have

resulted from ${}^9\text{Be}^* \rightarrow {}^9\text{Be} + \gamma$. The branching ratio, therefore, is the ratio of the number of ${}^9\text{Be}$ recoils detected to the number of ${}^9\text{Be}^*$ recoils produced.

For identification, the recoil ion was analyzed in rigidity, energy and velocity. This was done by sending the recoil along an 85-cm path through a low-resolution magnetic spectrometer to a surface-barrier detector (see Fig. 1). Furthermore, delayed coincidence was required between the recoil ion and the alpha particle from the formation reaction ${}^{11}\text{B}(d, \alpha){}^9\text{Be}^*$. The recoil nucleus was observed at 90° in the laboratory and the alpha particle was observed at the angle then determined by kinematics. Table 1 gives the kinematics relevant to the experiment. The alpha particles were identified by energy with a surface-barrier counter having a depletion depth thin enough that protons and deuterons gave pulse heights below the region of interest.

A 0.9- μA beam of 1.70-MeV deuterons from a Van de Graaff accelerator was used to bombard a thin natural-boron target evaporated on a thin backing of natural carbon. (Carbon-backed targets are able to withstand several times higher beam intensity than self-supporting boron targets.) The boron and carbon content of each target used is given in Table 2. A typical impurity composition for the targets in units of 10^{17} atom/cm² was ${}^{16}\text{O}$, 1.1; $25 \leq A \leq 30$, 0.3; $50 \leq A \leq 70$, 0.1; and $166 \leq A \leq 196$, 0.01. (See Appendix I and Figure 10)

A. Recoil-ion Detection

The alternating-gradient spectrometer indicated in Figure 1 has been described by Martin and Kraus (1957). The acceptance solid angle is 0.011 sr, but the entrance aperture is elliptical with the major

axis vertical, so that the width in the reaction plane is only 2.4° . The center of rotation of the target, the beam spot on the target, and the focus of the magnet were adjusted to coincide by bombarding a natural boron target with 1.17-MeV protons and moving the beam, the target chamber, and the entrance slit of the magnet to the position of maximum transmission of alpha particles from the reaction $^{10}\text{B}(p, \alpha) ^7\text{Be}^*$. The reaction rate was measured by counting gamma decays of the $^7\text{Be}^*$. The adjustment was complicated by the interaction of several of the adjustments and by the high accuracy required (moving vertically off center by 0.8 mm would reduce the counting rate by a factor of two). Several times during the adjustment the momentum profile of the magnet was checked. The magnet operated at full efficiency over a range of only 2.9% in $\Delta p/p$ compared to 5.0% obtained by Seeger (1963). There were no changes in the target chamber or magnet between this experiment and Seeger's experiment. Therefore, the difference in the momentum range presumably came from errors in positioning the beam spot with respect to the magnet focus which permitted some particles in the momentum range to hit the sides of the magnet. The range, however, was adequate for the recoil-ion detection. The magnetic field is measured by a torsion-balance fluxmeter, the current setting of which is inversely proportional to the rigidity.

The detector at the magnetic focus was an 11.4-mm circular gold-silicon surface-barrier detector with a counting area defined by a 3.2-mm slit. The pulse from the detector was amplified (as shown in the block diagram, Fig. 1) by a fast-amplifier system, clipped to 20-nsec width by a shorted length of 93Ω cable, and fed to both a co-

incidence mixer and to the lower beam of a Tektronix type 555 dual-beam oscilloscope, used for checking the adjustment of various circuits.

The pulse from the detector also went through a 1000 Ω resistor to a low-noise integrating preamp (Tennelec Model 100A). The signal was further amplified and stored on the horizontal side of a Nuclear Data two-dimensional pulse-height analyzer. A typical spectrum is shown in Fig. 2, corresponding to a magnet current setting of $EM/Z^2 = \text{energy} \times \text{mass}/(\text{charge})^2 = 4.46 \text{ MeV}$. Particle groups with different values of E and therefore different values of M/Z^2 are separated on this spectrum. Figure 2 shows peaks for α^+ and α^{++} ions. The positions where peaks from $^{11}\text{B}^{++}$ and $^9\text{Be}^{++}$ would appear with longer runs are also shown.

B. Alpha Detection

The chamber used in the experiment permits continuous variation of the alpha angle, θ_α . A 1-mm \times 5-mm slit, 16 mm from the target, defines the solid angle of the alpha counter, a 6-mm \times 10-mm gold-silicon surface-barrier detector. The long axes of the slit and counter are vertical.

The fast amplifiers for the alpha channel (shown in Fig. 1) are similar to those in the recoil-ion channel. A variable delay, however, has been added to delay the alpha pulse by the flight time required for the ^9Be recoil ion. The delay consisted of 77.7 m of RG114/U cable, which could be switch-selected from 0 to 255 units of 30.5 cm. Each 30.5-cm unit of cable corresponds to a delay of 1.2 nsec. The output of the fast amplifiers was fed to a coincidence mixer, the upper-beam input of the oscilloscope, and a biased amplifier.

Conventional slow electronics could not be used for the chamber-counter pulses since the intense flux of elastically scattered deuterons in the chamber counter would give an unacceptably high rate of pile-up pulses. Hence the fast pulses were fed to a biased amplifier set to pass only pulses higher than the deuteron pulses. The biased amplifier also stretched the pulses for storing on the vertical side of the two-dimensional pulse-height analyzer.

For identification of the various particle groups, the chamber counter spectrum was recorded with slow electronics (see Fig. 3). The groups were then identified by their energy (compared to a ThB alpha source). The counter bias was set such that protons with energy greater than 3.2 MeV penetrated the depletion layer.

After the various groups were identified, the biased amplifier was adjusted to pass pulses above about 2 or 3 MeV and the two-dimensional analyzer was adjusted to record pulses between about 4 MeV and 8 MeV (see Fig. 4 for such a spectrum).

C. Coincidence Detection

A tunnel-diode coincidence mixer was used in this experiment. A tunnel-diode at each input of the mixer, also served as a discriminator, set so that input pulses of half a volt were sufficient to trigger the diode from the low voltage to the high voltage portion of the characteristic curve. The ion and alpha pulses were clipped to 20 nsec. For a coincidence output, the ion and delayed alpha pulses had to occur within 20 nsec (for 0.5-volt pulses) to 40 nsec (for pulses above 0.7 volt). Both the ^9Be recoil ions and chamber alpha particles produced pulses of about one volt.

The fast rising coincidence output triggered the oscilloscope, and the "+ gate out" signal from the oscilloscope opened the coincidence gates of the multi-channel analyzer. When the coincidence gates were open, the two-dimensional analyzer stored the heights of the ion and alpha pulses.

D. Monitoring Equipment

An oscilloscope and five scalars monitored the operation of the electronics. The oscilloscope was used for making quick checks of the alpha and ion non-coincident spectra, to check amplifier gains and bias settings, and to check the coincidence circuit. The scalars counted the number of ion pulses through the slow electronics, the number of alpha pulses above about 6.5 MeV, the number of pulses firing the ion side of the coincidence mixer, the number of pulses that fired the alpha side, and the number of coincidence pulses.

E. Experimental Procedure

The subscripts 0, 1, and 2 will refer to quantities pertaining to reaction $^{11}\text{B}(d, \alpha)^9\text{Be}$ where the ^9Be is in the ground state, 1.7-MeV level, and 2.43-MeV level respectively. The subscript * can be replaced by either subscript 1 or 2. It is used to avoid repeating equations that hold for both the 1.7- and 2.43-MeV levels.

After positive identification of the prominent particle groups had been made on the basis of the non-coincident spectra (Figs. 2 and 4), the spectrometer current, the alpha-particle angle and delay were varied to obtain the maximum counting rate of $^9\text{Be}^{+++} - \alpha_0$ coincidences. The counting rates were usually normalized to 100 μC of beam on the target. The maximum $^9\text{Be}^{+++} - \alpha_0$ coincidence rate is called N_0 , oc-

curing at the fluxmeter setting I_0 , alpha angle Θ_0 , and the delay ℓ_0 . The number N_0 provides a measure of the coincidence efficiency which depends on the target thickness and on the slit defining the alpha counter acceptance.

After optimizing, the three parameters were changed to the appropriate values for ${}^9\text{Be}^{++} - \alpha_1$, ${}^9\text{Be}^{++} - \alpha_2$, or ${}^9\text{Be}^{++++} - \alpha_2$ events as follows:

	${}^9\text{Be}^{++} - \alpha_1$	${}^9\text{Be}^{++} - \alpha_2$	${}^9\text{Be}^{++++} - \alpha_2$
Fluxmeter current	$0.744 I_0$	$0.783 I_0$	$1.566 I_0$
Alpha delay	$\ell_0 + 7$ units (2.14 m)	$\ell_0 + 16$ units (4.87 m)	$\ell_0 + 16$ units (4.87 m)
Alpha angle	$\Theta_0 - 2.1^\circ$	$\Theta_0 - 3.1^\circ$	$\Theta_0 - 3.1^\circ$

The counting rate for any of these three groups of settings is called N_* . The change of delay and alpha angle is relatively small. The linearity of the fluxmeter was checked to 0.6% by observing various reaction groups from 1 - 6 MeV.

Runs of 2 to 4 hours with 0.9- μA beam intensity were made. The alpha energy and ion energy of each pair of coincidence pulses were stored in the two-dimensional pulse-height analyzer. The results of each run consisted of N_0 , and of N_* , determined from the analyzer output and from the integrated beam.

Figures 5 and 5A show the two-dimensional spectrum for a typical ${}^9\text{Be}^{++} - \alpha_2$ run on target No. 1 (see Table 2). The most prominent group, with an alpha energy of 5.3 MeV and ion energy of 1.5 MeV, is ${}^{11}\text{B}^{++} - \alpha$ coincidences from ${}^{13}\text{C}(d, \alpha){}^{11}\text{B}$ (the peak for the ${}^{11}\text{B}$ ions is shifted down from 1.6 MeV, probably because of energy loss in the boron layer of the target). The long ridge with an ion energy of 1.1 MeV

is due to α^+ - α coincidences from $^{10}\text{B}(d, \alpha) \rightarrow 3\alpha$ and $^{11}\text{B}(d, \alpha) \rightarrow 3\alpha + n$. The small peak from the desired reaction $^{11}\text{B}(d, \alpha_2)^9\text{Be}^{++}$, with alpha energy 5.3 MeV and ion energy 2.0 MeV, lies just above the ^{11}B recoil group. The separation between the ^{11}B recoil and ^9Be recoil groups from a longer run on target No. 1 is shown in Fig. 7, where the coincidences with alpha energy in the α_2 peak are summed and plotted as a function of ion energy. Target No. 1 had the highest C to B ratio, so the separation of the peaks was even better for the other targets. The group in Fig. 5 with ion energy 2.0 MeV and alpha energy 7.0 MeV results from the reaction $^{11}\text{B}(d, \alpha_0)^9\text{Be}^{++}$ where the ^9Be ion has lost enough energy in the target to go through the magnet. The separation between these stragglers and the desired group is shown in Fig. 8, for which seven runs totaling 21,540 μC have been summed. The tail of the straggler peak results in a small background under the $^9\text{Be} - \alpha_2$ peak. A measure of this background was made by setting the magnet for 2.19 MeV $^9\text{Be}^{++}$ ions and counting ions near that energy in coincidence with various alpha energies (see Fig. 9). The 1.7-MeV level in ^9Be should have contributed no more than one count to this run (estimated by multiplying the number if $^9\text{Be}^*$ (1.7-MeV level) produced at an angle where they could enter the magnet times the branching ratio for gamma decay of the 1.7-MeV level; see Sections III and IV). Finally, there is a small peak with ion energy 2.7 MeV and alpha energy 7.0 MeV. This group is presumed to be from $^{11}\text{B}(d, \alpha_0)^9\text{Be}$ with the ^9Be ion undergoing charge-exchange collisions with gas molecules near the center of the magnet that changed the charge of the ^9Be ion from $++$ to $+++$.

Figures 6 and 6A show the two-dimensional spectrum for the sum of six runs totaling 34,040 μ C with settings for $^{11}\text{B}(d, \alpha_1)^9\text{Be}^{++}$. Figure 6 is quite similar to Fig. 5 except the $^{13}\text{C}(d, \alpha)^{11}\text{B}$ group is quite weak and no (or perhaps one) count is in the $^{11}\text{B}(d, \alpha_1)^9\text{Be}^{++}$ group.

The $^{11}\text{B}(d, \alpha_2)^9\text{Be}^{++++}$ runs are also similar to Fig. 5 except the ridge of alpha coincidences is much stronger.

The number of counts obtained and the length of running for the coincidence measurements is given in Table 3.

III. ANALYSIS OF RESULTS

The ratio of $\Gamma_{\text{rad}}/\Gamma$ is the ratio of the rate of ${}^9\text{Be}^*$ surviving particle breakup (and hence observable) to the total rate of forming ${}^9\text{Be}^*$ (which is the total rate of producing α_* in the reaction). If B_* is the background rate and ϵ_* is the efficiency of the system for detecting excited-state coincidences, then

$$\begin{aligned} \frac{\Gamma_{\text{rad}}}{\Gamma} &= \frac{(\text{rate of observed } {}^9\text{Be}-\alpha_* \text{ coincidences}) - (\text{background rate})}{\epsilon_* \times (\text{rate of } \alpha_*)} \\ &= \frac{N_* - B_*}{\epsilon_* \alpha_*} \end{aligned} \quad (1)$$

The efficiency ϵ_o for detecting ground state coincidences can be found directly by experiment, since in this case all recoils survive:

$$\epsilon_o = \frac{(\text{rate of observed } {}^9\text{Be}-\alpha_o \text{ coincidences})}{\text{rate of } \alpha_o} = \frac{N_o}{\alpha_o} \quad (2)$$

By combining eqs. (1) and (2), we have

$$\frac{\Gamma_{\text{rad}}}{\Gamma} = \left(\frac{N_* - B_*}{N_o} \right) \left(\frac{\epsilon_o}{\epsilon_*} \right) \left(\frac{\alpha_o}{\alpha_*} \right) \quad (3)$$

This equation requires the ratio of coincidences for the excited state to those for the ground state, the ratio of the alpha particles associated with the two states, and the ratio of the detection efficiencies for the two states.

A. Counting Rate Factor $(N_* - B_*)/N_o$

The coincidence rates N_* were measured during each run as described in Section II. The background rate B_* is assumed proportional

to the number of counts in the straggler peak (see Section III E and Figure 9 for the method of background measurement). For the 2.43-MeV state, the background correction was less than 1% except for the short run on the thickest target, No. 2, for which it was 45%. Usually at the beginning and end of each run, N_o was measured, and the average value was used. The relative error for $(N_* - B_*)/N_o$ was then $[1/(N_* \text{ expected} + B_*) + (\Delta N_o/N_o)^2]^{1/2}$ where ΔN_o is half the difference of N_o measured at the beginning and end of the run. In several cases, N_o was not measured at the end of the run. In these cases, 30% was used for $\Delta N_o/N_o$. This is about $1\frac{1}{2}$ times the average value of $\Delta N_o/N_o$ found on runs where N_o was measured at both the beginning and end of the run. It is presumed that $\Delta N_o/N_o$ was so large because of changes in target wrinkling that affected counting efficiency.

For about 5% of the runs, N_o was measured by a scaler rather than with the two-dimensional analyzer. In these cases, N_o was corrected by the ratio of N_o (scaler)/ N_o (analyzer) averaged over the runs on the target where N_o was measured by the analyzer. This correction changed N_o by about 10% and contributed about 10% to the error of N_o . The difference between N_o (scaler) and N_o (analyzer) came mainly from counts in the tail (which were counted by the scaler) that were not in the rectangle over which the peak was summed (when counted with the pulse height analyzer).

For about 10% of the runs, the angle α_2 was not set correctly. The alpha acceptance angle was 3.6° , and the error in the alpha angle was never more than 1.2° . Since the coincidence rate for the ground state measured over a range of 6° each day, the effect of this small error in the alpha angle on efficiency was known. The correction to

the counting rate in these cases was about 10% with an error of about 6%.

B. Efficiency Factor

The efficiency factor ϵ_o/ϵ_* was broken into two factors

$$\frac{\epsilon_o}{\epsilon_*} = \left(\frac{t_o}{t_*} \right) \left(\frac{c_o}{c_*} \right)$$

Here, t_* is the fraction of the detected excited-state alpha particles whose accompanying ${}^9\text{Be}^*$ recoils have momentum within the spectrometer acceptance window; and similarly, t_o is the fraction of the ground-state group of ${}^9\text{Be}$ recoils within the spectrometer window, associated with detected alpha particles. The fraction of excited-state recoil ions in the charge state observed (2+ or 4+) is c_* , and the fraction of ground state recoil ions in the charge state observed (3+) is c_o .

To determine the charge state ratio of Be ions emerging from a boron foil, an elastic scattering experiment was done on foils having a layer of boron and a layer of Be. ${}^9\text{Be}$ ions from ${}^9\text{Be}(\alpha, {}^9\text{Be})\alpha$ emerging through the B layer were observed with a 61-cm double-focusing magnetic spectrometer. The charge-state ratios from these measurements at 1.78 and 2.52 MeV is given in Table 4. Tombrello and Bacher (1965) have measured the charge-state ratios at higher energies. Table 4 also gives the values of the charge-state ratios for 1.98, 2.19, and 2.73 MeV, interpolated by fitting Dmitriev functions to the data of this experiment and those of Tombrello and Bacher (Zaidens 1965). The error is estimated to be about 0.02 on each point. More information on the charge-state measurements is given in Appendix II.

The magnet efficiency as a function of rigidity was measured by observing ${}^9\text{Be}^{+++} - \alpha_0$ coincidences and varying magnet current. The efficiency profile was trapezoidal. It had a steep rise on the low energy side, was 2.9% wide on the top, and had a linear tail 2.1% wide on the high energy side. When the momentum width of the recoil group was greater than 2.9%, a correction was required to the counting efficiency.

One source of momentum broadening was energy loss due to finite target thickness, which was measured for each target by elastic scattering. Using the mean square charge of Be ions from Table 4, the energy loss of the ions was calculated (see Table 2) from the relation that dE/dx will be $\langle Z^2 \rangle$ times dE/dx for protons of the same velocity. Another source of momentum width was kinematical or $dE/d\theta$ broadening, including the extra width caused by deflection from gamma emission of the recoil ions into the magnet's geometrical aperture. The final source was the longitudinal component of the momentum of the emitted gamma ray. Isotropic distribution of the gamma ray was assumed. The three distributions were folded together and integrated with the magnet's efficiency profile. With all except target 2 (the thickest) the correction t_*/t_0 was less than 0.1% (see Table 5). If, due to wrinkling, the effective target thickness had been twice the amount determined from the elastic scattering, the the correction t_*/t_0 would have been less than 2% (except for target 2). However, measurements on the profile shape of the ground-state group showed the width to be equal to the assumed width to within 50%. For infinite target thickness (or the worst possible case of wrinkling), t_*/t_0 would be 1.4. For the 1.7-MeV level, no correction was needed since all runs were on the thinnest target, No. 5.

C. Population Factor α_*/α_0

To know the rate of producing recoil ions, the values of the ratios $\alpha_2(66.4^\circ)$ to $\alpha_0(69.5^\circ)$ and $\alpha_1(67.4^\circ)$ to $\alpha_0(69.5^\circ)$ were required. Figure 4 shows one of the alpha spectra that was used for measuring.

the ratios. The ratio of counts in the α_2 peak at 66.4° to counts in the α_0 peak at 69.5° was calculated with a least-square procedure which adjusted the height of three pairs of peaks centered on α_1 , α_2 , the next lower α peak (see Fig. 4), and the height of a constant background to give the best fit to the spectrum from about 5 MeV to 6.5 MeV. The α_0 peak from spectra at 69.5° (shifted down in energy an integer number of channels) were used to fit the three peaks. The α_0 peaks were used in pairs (one of which was shifted one more channel than the other) to simulate the effect of shifting down a fractional number of channels. The ratio of counts in the α_1 peak at 67.4° to counts in the α_0 peak at 69.5° was calculated in a similar manner. The following values were found:

$$\frac{\alpha_2(66.4^\circ)}{\alpha_0(69.5^\circ)} = 0.97 \pm 0.07 ,$$

$$\frac{\alpha_1(67.4^\circ)}{\alpha_0(69.5^\circ)} = 0.15 \pm 0.02 .$$

D. Calculations of $\Gamma_{\text{rad}}/\Gamma$

With all the terms of Eq. (3) now measured or calculated, the data were combined in the following way. For all runs on a charge state, $(N_* - B_*)/N_0$ was calculated and corrected by the thickness factor t_0/t_* . It is permissible to correct by t_0/t_* before averaging $(N_* - B_*)/N_0$ for all the runs on a target only because the error of t_0/t_* was much less than the final error of the experiment for all targets except target No. 2. The procedure is correct for target No. 2 because only one run was made on it. The error in t_0/t_* was assumed to be $1 - t_*/t_0$.

These numbers were then averaged with weighing factors $1/\text{error}^2$ for each term. This average value of $(N_* - B_*)t_o / N_o t_*$ was corrected by $1/c_*$, one piece of the charge state factor. For the measurement on the 2.43-MeV state (where measurements were made on two charge states) the values for the two charge states were now averaged with weighing factors $1/\text{error}^2$. Finally, the result was multiplied by the population factor α_o / α_* and the other piece of the charge-state factor c_o .

The immediate results of each run on the 2.43 MeV level are given in Table 6. Table 7 gives the intermediate calculations for the 2.43-MeV level. Table 8 gives the intermediate calculations for the 1.7-MeV level.

The results of the calculations are:

(2.43-MeV state)

$$\frac{\Gamma_{\text{rad}}}{\Gamma} = (1.16 \pm 0.14) \times 10^{-4}$$

(1.7-MeV state)

$$\frac{\Gamma_{\text{rad}}}{\Gamma} \leq 2.4 \times 10^{-5}.$$

IV. DISCUSSION

The limit of $\Gamma_{\text{rad}}/\Gamma \leq 2.4 \times 10^{-5}$ (63% confidence) measured for the 1.7-MeV level agrees with the value $(2.0 \pm 0.3) \times 10^{-5}$ obtained by dividing the gamma width of 4.5 ± 0.6 eV (Ngoc 1963) by the total width of 224 ± 25 keV (Kavanagh 1958).

The branching ratio $\Gamma_{\text{rad}}/\Gamma = (1.16 \pm 0.14) \times 10^{-4}$ obtained for the 2.43-MeV $5/2^-$ level may be combined with the gamma width of the level to obtain the total width. Inelastic electron scattering at 40 MeV indicates that the gamma width is 0.122 ± 0.015 eV (Edge 1962, Barber 1960). Dividing this value by the branching ratio gives a total width of 1.05 ± 0.18 keV.

The calculation of the gamma width from the inelastic electron scattering assumes that the $5/2^-$ level is the only level in ${}^9\text{Be}$ near 2.43 MeV (within about 50 keV). On the other hand, the $1/2^-$ level predicted by various models (Kunz 1960, Nilsson 1955, Kurath 1956) may be near the $5/2^-$ level. This level has not been seen but should show up in inelastic electron scattering. It is expected to have a total width of about 1/2 MeV. Since the $1/2^-$ level would have a very small value for $\Gamma_{\text{rad}}/\Gamma$ (about 10^{-6}) and since it has not been seen in ${}^{11}\text{B}(d, \alpha)$, it could not affect the measurement of $\Gamma_{\text{rad}}/\Gamma$ for the 2.43-MeV level by more than 5%. It would, however, lower the gamma width calculated from electron scattering by about 40%, and therefore lower the value we calculate for the total width.

The Nilsson model predicts the gamma width of the $5/2^-$ level to be 0.153 eV (see Appendix III), and intermediate coupling models predict the gamma width to be about 0.087 eV (Cohen 1965, Barker 1965).

This latter value for the gamma width combined with our value for $\Gamma_{\text{rad}}/\Gamma$ gives a total width of 0.75 keV.

The value $\Gamma = 1.05 \pm 0.18$ keV obtained from the measured gamma width divided by the branching ratio is in agreement with the measured upper limit, $\Gamma \leq 1$ keV (Gossett 1955). The total width is larger than the value 1/4 keV predicted by the alpha model (Henley 1960) (see Appendix III).

APPENDIX I

BORON FOILS

The experiment used thin natural boron foils. The foils were required to pass 2-MeV ^9Be ions at 45° with an energy loss of no more than 3% in order that most of the ^9Be recoils accepted at the entrance of the spectrometer would be counted. Also, the foils were required to be thin enough that straggler events (see Section II, E, page 9) did not interfere with the experiment. The foils were, however, made about as thick as the above considerations permitted, to maximize the counting rate. Targets that were $0.2\text{-}0.5 \times 10^{18}$ at/cm² thick were best for measurements on the 2.43-MeV level, while 0.2×10^{18} at/cm² was the best thickness for the 1.7-MeV level.

The procedure used to make thin boron foils by evaporating boron from a tantalum boat heated by electrical resistance is given below. The changes in procedure for making stronger foils with both a layer of carbon and a layer of boron follows. Finally, the boron-beryllium foils used for the Be charge state measurements are mentioned.

Select several clean microscope slides and brush any dust off the slide with a wad of fresh cotton. Vacuum evaporate BaCl_2 onto the slide (about 100 mg of BaCl_2 in a boat 30 cm from the slide). If the BaCl_2 is not dry, preheat it to 300°C in air before the vacuum evaporation. This will greatly reduce the amount of BaCl_2 that hops out of the boat during the evaporation.

Now wipe the BaCl_2 out of the bell jar. This will help keep the pressure down during the boron evaporation. Then mount a new, clean tantalum boat on the bell jar electrodes with copper hardware (a new

tungsten boat may also be used; experience in using both tantalum and tungsten boats for boron evaporation indicates that either type boat works as well as the other but that the tantalum boat is easier to make). The boat should be 0.25 mm by 8.5 mm by 60 mm and depressed in the center so the boron won't flow out. From 50 to 100 mg of boron should be piled along the center of the boat with strips 1 to 2 mm wide along each edge of the boat left free of boron. Leaving the strips free of boron helps prevent the boat from breaking before the evaporation is complete.

Place the slides with the BaCl_2 layer 10 cm above the boat and re-evacuate the bell jar. Shield the microscope slides from the boat and heat the boat slowly to a dull red heat, driving the water off the boron. Then raise the temperature to a bright yellow white for two minutes to drive off additional impurities. It is best to then let the boat cool for five minutes. Finally, heat the boat to the evaporating temperature over a period of about one minute. The evaporating temperature produces a bright white light similar in color to a new 500-watt light bulb. At the evaporating temperature rapid eddies can be seen in the liquid boron (use dark goggles to look). As the boron alloys into the tantalum, it is necessary to continue raising the heating voltage in order to maintain the boat temperature. The evaporation should continue until enough or all of the unalloyed boron has been evaporated. When all of the unalloyed boron has evaporated, the color of the boat becomes brighter, bluer and more uniform. To minimize the chance of boat breakage, the evaporation should be completed fairly rapidly, with the boat remaining at the evaporation temperature no longer than two minutes.

Once the slides have cooled they may be removed from the bell jar and stored until one wants to float the foils from the slides. No

difference in physical properties or chemical composition was noticed in foils stored on the slides for up to six months.

To float the foils from a slide, scribe lines dividing the foil into squares (1.3 cm squares were used). Support the slide at 10° in a dish and slowly syphon water into the dish. If cracks appear in the foils as they float off, reduce the rate of rise of the water level. If the foils do not float off with the water level rising at 2 mm/hr, it is best to make a new batch of foils.

Once all the foils have floated off a slide, each foil may be pulled vertically out of the water with a clean tantalum holder. If the foil does not break upon drying, it will probably last until it receives some rough treatment. Perhaps one-quarter of the boron foils may be expected to survive the floating operation.

The composition of the foils was measured by counting elastically scattered 1-MeV protons at $\Theta_{\text{lab}} = 150^\circ$ with the 27-cm double-focusing spectrometer. For this spectrometer the number of atoms/cm², A , is determined by the number of counts from 9.28 μC of beam, N_q , at fluxmeter current I and by the elastic-scattering cross-section $d\sigma/d\Omega$. The formula given by Seeger (1963) is

$$A = \frac{3.43 \times 10^{18}}{\frac{d\sigma}{d\Omega}} \int \frac{N_q(I)}{I} dI .$$

The following elastic-scattering cross sections were used:

- B^{10} : 70 mb/ster (Overley 1961)
- B^{11} : 80 mb/ster (Tautfest 1955)
- C^{12} : 188 mb/ster (Jackson 1953)

N^{14} : 109 mb/ster (Tautfest 1955)

O^{16} : 154 mb/ster (Eppling 1953)

The Rutherford cross-section was used above mass 16. The following variations (in units of 10^{17} at/cm²) of composition were found from measurements on 12 boron and carbon-boron foils:

B: 5 - 12

C: 0.7 - 0.8 no carbon added

C: 3 - 5 carbon layer added

O: 0.6 - 1.8

25 < A < 30 (presumably Si): 0.02 - 0.3

50 < A < 70 (presumably Fe): 0.05 - 0.2

166 < A < 196 (presumably Ta): 0.01 - 0.02 .

No difference in impurity content was noted between the boron and carbon-boron foils. Some foils may have shown a trace (less than 10^{-15} at/cm² unless noted) of masses near the following masses: N (5×10^{-15} at/cm²), F, Na, S, Cl, and Ba. The composition and proton spectrum from one boron foil are shown in Fig. 10. Since the variation in the various impurities was too small to affect the branching ratio measurement, only the boron and carbon content of the foils used in the experiment was measured.

Most of the boron foils would break at beam currents of 0.1 to 0.2 μ A of 1 MeV protons.

The strength of foils with a carbon layer is much greater. Such targets are easier to float and will withstand 1-2 μ A of 1-MeV protons for an 1-5-mm by 3-mm beam spot. At least 80% of them will survive the floating procedure.

Targets with a carbon layer are made like those without one, except a layer of carbon is added either before or after the boron evaporation. The carbon should be deposited from a blue arc between spectroscopically pure carbon electrodes. If the carbon-boron foils are mounted on clean target holders, they will often curl up and roll off at the slightest touch. With a little finger grease on the target holder, the foils are somewhat harder to mount, but once dry they stick to the holder better.

Foils were also made with a layer of beryllium over a boron layer. These foils were made by evaporating beryllium onto the boron and then floating. The resulting foils were quite weak and would withstand about a 30-nA beam of 10-MeV alphas for an 1.5 mm by 3-mm beam spot.

Appendix II

BERYLLIUM CHARGE-STATE RATIOS

Since only two of the charge states of the ^9Be recoils were observed during the branching-ratio measurement, it was necessary to measure the probability of producing Be ions in these two charge states. This was done by bombarding beryllium-boron foils with 7.07-MeV and 9.74-MeV alpha particles from the C.I.T. tandem and counting the ^9Be recoils from the reaction $^9\text{Be}(\alpha, ^9\text{Be})$ at 55° with the 16-counter array in the 61 cm spectrometer. The target was positioned so that the Be recoils passed through the boron layer before going into the magnet.

Measurements were made with recoil energies of 1.78 MeV and 2.52 MeV. The ions were produced at 1.98 MeV and 2.73 MeV, but some energy was lost in the boron layer of the target. Usually, for each charge-state several runs were made that completely covered the recoil peak (see Figs. 11 and 12). Measurements were not made, however, for the $1+$ charge-state at 2.52 MeV or the lower energy end of the $4+$ charge-state peak at 1.78 MeV because of difficulty in operating the fluxmeter of the magnet.

The combination of rigidity measurement by the magnetic spectrometer and energy measurement by the solid-state counters in the array permitted separation of the $1+$, $2+$, and $4+$ ^9Be recoils from other reaction products. The $3+$ recoils, however, could not be separated from protons and alphas. From observations made a short distance either side of the $3+$ recoil peak, it appeared that the peak sat on a constant background of about 5% of the height of the peak. This background probably consisted of alpha stragglers.

For analyzing the data, a method that compared the shapes of the various recoil peaks was used. The recoil peaks should all have the same shape except for variations caused by such things as counting statistics, backgrounds from other reactions (important for the 3+ charge state), and erratic counter operation (it appears that a few of the points are lower than one would expect from statistics). The numbers A_{ij} and B_{ij} were adjusted to give the best least-squares fit to the relations

$$N_i(E) \approx A_{ij} N_j(E) + B_{ij}$$

(i and j run over all the charge states observed).

The number of counts observed at recoil energy E for charge-state i times the counter efficiency factor is $N_i(E)$. The same quantity for charge state j is $N_j(E)$. The counter efficiency corrections (up to $\pm 10\%$), measured by Lew Cocke (1964) are given in Table 9. The ratio of ions in charge-state i to those in charge-state j is then A_{ij} and the difference in any constant background under the two peaks is B_{ij} . A nonconstant background will increase the error calculated for A_{ij} and B_{ij} above that expected from counting statistics. The values obtained for A_{ij} are given in Table 10. The B_{ij} were all zero except when i or j was 3.

The fraction R_i of ions in charge state i can be written as

$$R_i = r_i / \sum_j r_j,$$

$$r_i = \frac{1}{\sum_j A_{ji}}.$$

The second equation gives the expected value of the charge-state ratio

when there is no error in the A_{ji} . The first equation requires that probability that the ion in one of the charge-states be one. The $\sum_i x_i$ over all charge states may not be exactly one when there are errors in the original data because in this case the least-squares procedure does not, in general, give $A_{ij} = 1/A_{ji}$. This defect of the least-squares procedure is not serious so long as the errors are not large. The fraction of ions in each charge-state, along with the calculated error, is given in Table 4.

The values for the charge-state ratios agree with those obtained by dividing the counts in each peak (after subtracting a constant background for the 3+ charge-state) by the number of counts in all the peaks. This simple procedure, however, permits calculation only of the errors from counting statistics, which are only about 0.3%. Therefore, the more complicated method was used since it gave a better indication of the error in the experiment.

Appendix III

CALCULATION OF PARTICLE AND GAMMA WIDTHS FOR
THE 2.43-MeV LEVEL IN ${}^9\text{Be}$

The gamma width of the 2.43-MeV level of ${}^9\text{Be}$ may be calculated from the Nilsson model. First one uses the ground-state magnetic moment μ to calculate the g-value, g_R , associated with the collective angular momentum, with the formula

$$\mu = \frac{J}{J+1} \left[g_\ell J + g_R + \frac{1}{2} (g_s - g_\ell) \sum_\ell \left(a_{\ell, K-\frac{1}{2}}^2 - a_{\ell, K+\frac{1}{2}}^2 \right) \right]$$

(Preston 1962).

For the calculation we use the ground-state spin, $J = 3/2$, the odd neutron orbital g-factor, $g_\ell = 0$, the neutron g-factor, $g_s = -3.8263$ (Preston 1962), and the Nilsson ${}^9\text{Be}$ wave function, $a_{1, 3/2 - 1/2}^2 = 1$ and all other $a^2 = 0$ (Nilsson 1955). Using $\mu_{{}^9\text{Be}} = -1.177 \pm 0.001 \text{ nm}$ (Preston 1962) and solving for g_R we get

$$g_R = -0.048 .$$

The gamma width is given by

$$\Gamma = T(M1) = \frac{16\pi}{9} k^3 \mu_0^2 (g_K - g_R)^2 K^2 \frac{(J-K)(J+K)}{J(2J+1)}$$

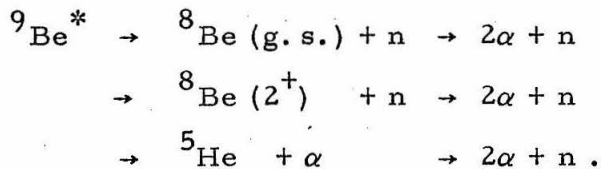
(Preston 1962).

Here $T(M1)$ is the transition probability per unit time for M1 decay, $k = E/\hbar c$, the gamma decay energy divided by $\hbar c$, μ_0 is the nuclear magneton,

$$g_K = g_\ell + \frac{1}{2K} (g_s - g_\ell) \left(\sum_\ell (a_{\ell, K-\frac{1}{2}}^2 - a_{\ell, K+\frac{1}{2}}^2) \right)$$

($= -1.2754$ for ${}^9\text{Be}$), $K = 3/2$, the projection of the total angular momentum on the intrinsic nuclear axis, and $J = 5/2$, the total angular momentum. Using these values the formula gives $\Gamma_\gamma = 0.153 \text{ eV}$.

The 2.43-MeV level of ${}^9\text{Be}$ can decay into two alpha particles plus a neutron in the following ways:



The decay through ${}^8\text{Be} (\text{g. s.}) + n$ requires f-wave neutrons. This decay is forbidden in the shell model but is permitted in the Nilsson model and in the alpha model (Henley 1960). Marion (1959) has measured the branching ratio for this decay and finds that it accounts for 0.12 ± 0.05 of the decay. The first excited state of ${}^8\text{Be} + n$ is 2.1 MeV above the 2.43-MeV level in ${}^9\text{Be}$, but since the level is 1.45-MeV wide, the decay may proceed through the tail of the level. The ground state of ${}^5\text{He} + \alpha$ is 100 keV above the 2.43-MeV level of ${}^9\text{Be}$, and is 577-keV wide, so the decay may also proceed through the tail of this level. The energies and widths are from Lauritsen (1965). The decay through ${}^8\text{Be} (2^+) + n$ and ${}^5\text{He} + \alpha$ become identical if neutron recoil effects are neglected. It is not safe, therefore, to consider these two decay modes as independent unless one of them gives a much larger decay probability than the other (Henley 1960).

The partial width for each decay mode can be estimated from

$$\Gamma = 2\gamma^2 \frac{\int_0^{E_{\text{avail}}} P_\ell(E) \rho(E_{\text{avail}} - E) dE}{\int_{-\infty}^{\infty} \rho(E) dE}$$

where E_{avail} is the energy to go from the initial level to the final products, $P_\ell(E)$ is the penetrability of the first particle emitted (with angular momentum ℓ and energy E , and $\rho(E)$ is the density of states

available in the intermediate nucleus (^8Be or ^5He). The reduced width γ^2 , can be expressed as

$$\gamma^2 = \frac{3}{2} \frac{\hbar^2}{mR^2} s \Theta_{sp}^2$$

where m is the reduced mass of the emitted particle, R is the interaction radius, s is the spectroscopic factor, and Θ_{sp}^2 is the dimensionless reduced width.

The spectroscopic factor for a nucleon or alpha decay of a p-shell nucleus is given by

$$s = \sum_x \left| \frac{\Theta_x(TJM_T, \bar{T}\bar{J}\bar{M}_T)}{\Theta_{sp}} \right|^2$$

$$\text{where } \frac{\Theta_x}{\Theta} = n^{\frac{1}{2}} \left(\bar{T}\bar{T}\bar{M}_T M_T - \bar{M}_T \right) \left| T M_T \right> \times$$

$$\sum_{\substack{[\lambda]SL \\ [\bar{\lambda}]\bar{S}\bar{L}}} \left(a([\lambda]TSL) \bar{a}([\bar{\lambda}]\bar{T}\bar{S}\bar{L}) \times \right.$$

$$\left. (-)^{\bar{J} - S - \bar{S} + x} U(\bar{L}\bar{S} \times \bar{S}, \bar{J}S) U(S\bar{L}J\bar{L}, x L) \times \right.$$

$$\left. \left(1p^n[\lambda]TSL \right) \left\{ 1p^{\bar{n}}[\bar{\lambda}]\bar{T}\bar{S}\bar{L}, 1p^{n - \bar{n}} \right\} \right)$$

(Barker 1965, Lane 1960)

Symbols with no bars refer to the initial nucleus, symbols with one bar refer to the intermediate nucleus, and symbols with two bars refer to the nucleon or alpha particle. The number of p-shell nucleons is n , T is the isotopic spin, J is the total angular momentum, M_T is projection of the isotopic spin ($(N - Z)/2$ a is the coefficient in the

LS expansion of the initial nucleus, $[\lambda]$, L, S are the partition, orbital angular momentum, and spin of a state S in which the initial nucleus is expanded, the U-coefficient is given in Rotenberg (1959), and $\langle |j\rangle$ is the fractional parentage coefficient. For Barker's (1965) wave functions $s(^9\text{Be} \rightarrow ^8\text{Be}(2^+) + n) = 1.11$. In the LS limit (where $\psi_9(^9\text{Be}) = \psi(1s^4 1p^5 [41] \frac{1}{2} \frac{1}{2} 2, \frac{5}{2})$ and $\psi_8(^8\text{Be}) = \psi(1s^4 1p^4 [4] 0 0 2, 2)$) $s = 1.25$. The LS limit gives $s(^9\text{Be} \rightarrow ^5\text{He} + \alpha) = 7/9$. Barker's wave functions do not permit calculations of the decay through ^8Be (g. s.).

Calculation of Θ_{sp}^2 requires evaluation of the nuclear wave function at the nuclear surface. Since the simple models with infinite well depths do not provide a good value for Θ_{sp}^2 , it is usually treated as a parameter and adjusted to fit the known decay widths. Barker (1965) has fit many decays of light nuclei with Θ_{sp}^2 (p wave nucleon) = 0.3 and Θ_{sp}^2 (f-wave alpha) = 0.4 using $1.45 (A_1^{1/3} + A_2^{1/3}) \times 10^{-13}$ cm as an interaction radius where A_1 and A_2 are the mass numbers of the two decay products.

For the density of states factor one could use $\rho(E) = \sin^2(\delta_\ell + \phi_\ell)$ where δ_ℓ is the nuclear phase shift and ϕ_ℓ is the negative of the hard-sphere phase shift (for scattering of the two decay products of the intermediate level), except that the α - α d-wave and α -n $P_{3/2}$ phase shifts have not been measured at the energies important to this decay. At these low energies δ_ℓ approaches $-\phi_\ell$ and therefore it is difficult to make a useful measurement of $\delta_\ell + \phi_\ell$. One can, however, fit the data at higher energies with a single-level formula. One then has (Barker 1962)

$$\rho(E) = \frac{\Gamma_{\ell}(E)}{(E_{\ell} + \Delta_{\ell}(E) - E)^2 + \frac{1}{4} \Gamma_{\ell}^2(E)},$$

where $\Gamma_{\ell}(E) = 2\gamma_{\ell} P_{\ell}(E)$ is the width of the intermediate level, $\Delta(E)$ is the coulomb level shift, and $E_{\ell} + \Delta_{\ell}(E_r) = E_r$ is the energy available for decay of the intermediate level. Since the 2.43-MeV level of ${}^9\text{Be}$ is below the resonant energy for decay through both ${}^5\text{He} + n$ and ${}^8\text{Be}(2^+) + n$, the density of states function is quite sensitive to its parameters. Also, there are no phase-shift data in the relevant energy range to compare with.

The width of the ${}^9\text{Be}$ 2.43-MeV level was calculated using an interaction radius in ${}^9\text{Be}$ of $1.45 \times (A_1^{1/3} + A^{1/3}) \times 10^{-13}$ cm (4.35 f for ${}^5\text{He} + \alpha$ and 4.78 f for ${}^8\text{Be}(2^+) + n$) with various sets of parameters for the single level formula. The results of calculations with parameters from phase shift data and with parameters from the average of many measurements the energy and width of the intermediate levels are given in Table 11. For the parameters from the average values, various interaction radii for the decay of the intermediate levels were used in the calculation to show the sensitivity of the calculations to variations in this parameter. The calculated widths are also sensitive to variations of E_r and $\Gamma(E_r)$. No reasonable variations of these parameters can raise the calculated width to the value of the measured width (1.16 ± 0.14 keV).

The alpha model (Henley 1960) for ${}^9\text{Be}$ interaction radii of 1.45 $(A_1^{1/3} + A_2^{1/3}) \times 10^{-13}$ cm predicts the following widths $\Gamma_{8\text{Be}(2^+)+n} = 7$ eV, and $\Gamma_{8\text{Be}(g.s.)+n} = 57$ eV (see Table). The alpha-model calculations use finite-depth nuclear wells. Henley (1960), therefore,

could evaluate the nuclear wave functions at the nuclear surface and did not have a parameter corresponding to Θ_{sp}^2 .

List of References

- Barber, W. C., Berthold, F., Fricke, G., and Gudden, F. E. 1960, Phys. Rev. 120, 2081.
- Barker, F. C., and Treacy, P. B. 1962, Nuclear Phys. 38, 33.
- Barker, F. C. 1965, private communication. The wave functions Barker used for ^9Be and ^8Be will be published in Nuclear Phys.
- Cocke, C. L. 1964, private communication.
- Cohen, S. and Kurath, D. 1965 (to be published).
- Dodder, D. C. and Gammel, J. L. 1952, Phys. Rev. 88, 522.
- Edge, R. D. and Peterson, G. A. 1962, Phys. Rev. 128, 2750.
- Eppling, F. J., et al. 1953, Phys. Rev. 91, 438A.
- Gossett, C. R., Phillips, G. C., Schiffer, J. P., and Windham, P. M. 1955, Phys. Rev. 100, 203.
- Henley, E. M. and Kunz, P. D. 1960, Phys. Rev. 118, 248.
- Jackson, H. L., et al. 1953, Phys. Rev. 89, 365.
- Kavanagh, R. W. and Barnes, C. A. 1958, Phys. Rev. 112, 503, and private communication. A re-examination of the original data has revealed a calculation error affecting the values quoted for the widths of the 1.75- and 3.02-MeV states: The correct values are $\Gamma_{1.75} = 224 \pm 25$ keV and $\Gamma_{3.02} = 257 \pm 25$ keV.
- Kunz, P. D. 1960, Ann. Phys. 11, 275.
- Kurath, D. 1956, Phys. Rev. 101, 216.
- Lane, A. M. 1960, Rev. Mod. Phys. 32, 519.
- Lauritsen, T. and Ajzenberg-Selove. 1965 (to be published in Nuclear Phys).
- Lucas, B. T., Cospser, S. W., and Johnson, O. E. 1964, Phys. Rev. 133, B963.
- Marion, J. B., Levin, J. S., and Cranberg, L. 1959, Phys. Rev. 114, 1584.
- Martin, H. J. and Kraus, A. A. 1957, Rev. Sci. Inst. 28, 175; also, Martin, H. J. 1956, Thesis, California Institute of Technology.

- Nilsson, S.G. 1955, Kg. Dan. Vid. Selsk. Mat. Fys. Medd. 29,
No. 16.
- Ngoc, H.N., Hors, M., and Perez y Jorba, J. 1963, Nuclear Phys.
42, 62.
- Overley, J.C. 1961, Thesis, California Institute of Technology.
- Preston, M.A. 1962, Theory of the Nucleus, Addison-Wesley,
Palo Alto, pp. 62, 152, 329, 340.
- Renkin, J.H. 1963, Thesis, California Institute of Technology.
- Rotenberg, M., Bivins, R., Metropolis, N., Wooten, J.K., Jr.
1959, The 3-j and 6-j Symbols, the Technology Press,
Cambridge, Mass.
- Russell, J.L., Jr., Phillips, G.C., and Reich, C.W. 1956, Phys.
Rev. 104, 135.
- Seeger, P.A. 1963, Thesis, California Institute of Technology.
- Tautfest, G.W. and Rubin, S. 1956, Phys. Rev. 103, 196.
- Tombrello, T.A. and Bacher, A.D. 1965 (to be published in Ref. 21).
- Zaidins, C.S. 1965 (to be published).

Table 1

Kinematics (See Pg. 3) $(E_d = 1.7 \text{ MeV})$

Recoil Ion	Ion Recoil Energy (MeV)	Δt (n sec) for 85 cm	Alpha Energy (MeV)	Θ_α (deg)
^9Be (ground)	2.730	111	6.997	69.5
$^9\text{Be}^*$ (1.7 MeV)	2.191	123	5.786	67.4
$^9\text{Be}^*$ (2.43 MeV)	1.982	130	5.314	66.4
^{11}B (ground)	1.604	159	5.263	66.2

Table 2

Target Thicknesses and Energy-loss Data for ^9Be Ions
 (See Pgs. 3 and 14.)

Target Number	Thickness		$\Delta E/E$	
	B(10^{18} at/cm 2)	C(10^{18} at/cm 2)	1.98 MeV	2.73 MeV
1	0.42	10	0.83%	0.58%
2	0.96	12	1.89%	1.33%
3	0.39	0.50	0.77%	0.54%
4	0.44	1.28	0.87%	0.61%
5	0.21	0.66	0.41%	0.28%

Table 3Summary of Experimental Results (See Page 10.)

Coincidence Type	Counts	μ Coulombs of beam on target
${}^9\text{Be}^{++} - \alpha_2$	361	61530
${}^9\text{Be}^{++++} - \alpha_2$	23	32900
${}^9\text{Be}^{++} - \alpha_1$	0	42040

Table 4Charge-State Fractions for ^9Be (See Pgs. 13 and 24.)

	Measured		Calculated*		
	1.78 MeV	2.52 MeV	1.98 MeV	2.19 MeV	2.73 MeV
+1	0.0476 ± 0.005	0.013	0.03	0.02	0.01
+2	0.467 ± 0.012	0.298 ± 0.013	0.40	0.36	0.27
+3	0.428 ± 0.009	0.560 ± 0.025	0.47	0.51	0.55
+4	0.057 ± 0.01	0.139 ± 0.006	0.10	0.11	0.17

*Error of ± 0.02 assumed for each point.

Table 5Thickness Factors (See Pg. 14.)

Target	t_2 (1.98 MeV)	t_o (2.73 MeV)	t_*/t_o
1	0.999	1.000	0.999
2	0.971	0.992	0.981
3	0.999	1.000	0.999
4	0.999	1.000	0.999
5	1.000	1.000	1.000

Table 6 - Initial Data From Each Run (See Pgs. 11 and 41.)

Coincidences with ^9Be in 2+ Charge-State

N	DATE	T	C	STR	RNLN	BCCNT	BE	AE	BCLN	ECCNT	EE	EA	ECLN	R	RER
1	5-07	1	23	59	557A	5462	90	94	120A	6995	S	S	87A	72	22
2	5-08	1	6	7	30	6811		93	10	S		S	S	58	47
3	5-09	1	14	22	40	13867	92	92	30	S	S	S	S	78	27
4	5-10	1	11	49	560A	4420		86	69A	11246	89	S	203A	33	47
5	5-13	1	24	25	478A	3802		AV	70A	8262	90	AV	135A	91	19
6	5-13	1	53	51	824A	8262	S	AV	135A	14253	S	AV	199A	107	14
7	5-14	1	28	42	554A	4048			70A	3900	89		63A	88	18
8	5-14	1	71	54	1000A	S	S		S	8041	S		113A	120	12
9	5-28	2	18	762	375A	42114			727A	20282			407A	49	47
10	5-30	3	13	2	400A	18834			411A	7404	72		20A	90	37
11	6-04	4	11	46	326	12509			30	20446	82		67	97	37
12	6-04	4	8	190	290	19715			58	24511			58	54	52
13	6-05	4	13	105	290	30604			58	25037			58	85	30
14	6-05	4	7	116	290	24654			58	25076			58	46	55
15	6-05	4	12	123	290	25129			58	22741			58	89	30
16	6-05	4	10	176	348	19634			58	19009			58	70	38
17	7-02	4	15	133	320	12358			58	12181			58	139	21
18	7-06	4	6	45	171	11577			58	S			S	100	38
19	7-24	5	5	0	400	4710			40	4383			40	110	39
20	7-26	5	4	2	800	4690			40	3364			40	49	66
21	7-27	5	2	6	400	3886			40	2901			40	57	87
22	7-27	5	1	4	440	S			S	1459			40	40	149
23	7-28	5	3	3	240	5242			40	3910			40	108	52
24	7-29	5	3	8	800	4237			40	3198			40	39	85

40

Coincidences with ^9Be in 4+ Charge-State

N	DATE	T	C	STR	RNLN	BCCNT	BE	AE	BCLN	ECCNT	EE	EA	ECLN	R	RER
1	7-02	4	8	19	800	AN			AN	AN			AN	31	30
2	7-03	4	4	8	800	15653			40	11281			40	15	64
3	7-03	4	2	15	400	S			S	11242			40	16	85
4	7-04	4	4	6	480	14409			40	10509			40	26	49
5	7-06	4	5	5	810	11825			40	11577			40	21	46

Table 6 Headings

- N - Number to identify each run.
- DATE - Date of run.
- T - Target number (See Table 2 for the thickness of each target).
- C - Number of coincidence counts with the correct energies for excited states events (See Fig. 5 and Pg. 8).
- STR - Number of coincidence counts with the correct energies for ground state straggler events (See Fig. 8 and Pg. 9).
- RNLN - Length of the run in which C and STR are measured. This run length is in units of $10\mu\text{C}$. of beam unless A appears after the number. In the latter case the units are 10,000 α counts.
- AE - Percent correction for alpha angle error. During some runs the angle of the alpha counter was 0.7° or 1.2° too large while measuring excited state coincidences (the counter opening was 3.6°). (During the calibration run ($\text{Be}^{9+++}-\alpha_0$) the coincidence efficiency was measured at 1° steps. AE is 100 times the calibration coincidence rate at the correct angle 0.7° (or 1.2°) divided by the calibration rate at the correct angle.
- B - All symbols starting with B refer to measurements of the calibration rate (counting $\text{Be}^{9+++}-\alpha_0$) made at the beginning of the run (See Pg. 8).
- BCCNT - Number of coincidences for the calibration reaction.

- BE - Percent efficiency for counting BCCNT. For the runs where BCCNT was counted with a scalar, it was necessary to correct BCCNT since some coincidences counted by the scalar did not have the correct energy for events from the calibration reaction ($\text{Be}^{9+++} - \alpha_0$). At least once each day this ratio was checked by measuring the number of counts with the two dimensional analyzer and the scalar BE is 100 times the analyzer counts (which have the correct ion and alpha energy) divided by the scalar counts (all coincidences).
- BCLN - Length of the run in which BCCNT was measured. This run length is in units of $10\mu\text{C}$ unless A appears after the number. In the latter case the units are 1,000 α counts.
- E - All symbols beginning with E refer to measurements of the calibration coincidence rate made at the end of the run. These symbols have the same meaning as the corresponding symbols starting with B.
- R - The ratio of the excited-state coincidence counting rate to the ground-state coincidence counting rate after applying the corrections given in this table. Let $R^* = (C - 0.0106 \times \text{STR}) / (\text{RNLN} \times (\text{AE}/100))$. $\text{BR} = \text{BCCNT} \times (\text{BE}/100) / \text{BCCLN}$, $\text{ER} = \text{ECCNT} \times (\text{EE}/100) / \text{BCCLN}$ and $\text{GE} = (\text{BR} + \text{ER})/2$. Then $R = R^*/\text{GE}$. (See Pg. 15).
- RER - The percent error in R (see pg. 15 for a discussion of error calculations).

Table 6 Symbols

- blank - The correction factor (SE, Be, or EE) was not needed.
One may use 100% for its value in any formula.
- A - The length of the run was measured by counting the number of alphas with energy above about 6.5 MeV. Then the units are 10,000 α for RNLN and 1,000 α for BCLN and ECLN.
- AN - No measurement of the calibration rate was made for this run. The average calibration rate from all other runs on this target was used for this run.
- AV - No measurement of the correction for the alpha angle was made this day. The average of all other measurements was used.
- S - Use the value from the previous calibration run (the order is beginning calibration, run 1; end calibration, run 1; beginning calibration, run 2; etc.). When the calibration was not checked at the end of the run, the calibration error was considered to be 1.5 times the average of measured calibration variations.

Table 7

Calculations of 2.43-MeV State (See Pg. 11.)

+2 Charge State

Target	$\frac{(N_2 - B_2)}{N_o} \times \frac{t_o}{t_2} \times 10^4$	Target	$\frac{(N_2 - B_2)}{N_o} \times \frac{t_o}{t_2} \times 10^4$
1	0.76 ± 0.28	4	0.86 ± 0.26
1	0.63 ± 0.32	4	0.46 ± 0.26
1	0.85 ± 0.26	4	0.89 ± 0.27
1	0.39 ± 0.18	4	0.70 ± 0.27
1	1.15 ± 0.18	4	1.39 ± 0.29
1	0.89 ± 0.16	4	1.00 ± 0.39
1	1.20 ± 0.15	5	1.10 ± 0.42
2	0.49 ± 0.23	5	0.49 ± 0.33
3	0.90 ± 0.33	5	0.57 ± 0.50
4	0.97 ± 0.37	5	0.40 ± 0.60
4	0.54 ± 0.28	5	1.08 ± 0.57
		5	0.39 ± 0.33

$$\text{average } \frac{(N_2 - B_2) t_o}{N_o t_2} = (0.825 \pm 0.063) \times 10^{-4}$$

+4 Charge State

Target	$\frac{(N_2 - B_2)}{N_o} \times \frac{t_o}{t_2} \times 10^4$	Target	$\frac{(N_2 - B_2)}{N_o} \times \frac{t_o}{t_2} \times 10^4$
5	0.31 ± 0.09	5	0.16 ± 0.14
5	0.15 ± 0.09	5	0.26 ± 0.13
		5	0.20 ± 0.10

$$\text{average } \frac{(N_2 - B_2) t_o}{N_o t_2} = (0.220 \pm 0.047) \times 10^{-4}$$

Table 7 (cont'd.)

charge	$\frac{N_2 - B_2}{N_o} \frac{t_o}{t_2} \frac{1}{c_2} \times 10^4$
+2	20.5 ± 1.9
+4	22.4 ± 6.6
average	20.6 ± 1.8

$$\begin{aligned}
 \frac{\Gamma_{\text{rad}}}{\Gamma} &= \left(\frac{N_2 - B_2}{N_o} \frac{t_o}{t_2} \frac{1}{c_2} \right) \times \frac{c_o}{1} \times \frac{\alpha_o}{\alpha_2} \\
 &= (20.6 \pm 1.8) \times 10^{-4} \times (0.55 \pm 0.02) \times (0.972 \times 0.072)^{-1} \\
 &= (1.16 \pm 0.14) \times 10^{-4}
 \end{aligned}$$

Table 8

Calculation of Limit on $\Gamma_{\text{rad}}/\Gamma$ for 1.7 MeV State

(See Pg. 11.)

Target	No. of Runs	Total Length	$\frac{\text{Be}^{9*} \text{ Counts}}{\mu\text{C}}$	$\frac{\text{Be}^9 \text{ Counts}}{\mu\text{C}}$
5	7	42040 μC	0	10.13

$$\frac{N_1}{N_2} = 0 \pm \frac{1}{10.13 \times 42040} \quad (0 \pm 2.3) \times 10^{-6}$$

$$\frac{\Gamma_{\text{rad}}}{\Gamma} (1.7) = \frac{N_1}{N_0} \times \frac{t_0}{t_1} \times \frac{c_0}{c_1} \times \frac{\alpha_0}{\alpha_1}$$

$$= (0 \pm 2.3) \times 10^{-6} \times 1 \times \frac{0.55 \pm 0.02}{0.36 \pm 0.02} \times (0.15 \pm 0.02)^{-1}$$

$$\leq 2.4 \times 10^{-5}$$

Counter Correction Factors[†] (See Appendix II, Pg. 21.)

<u>Counter Number</u>	<u>Factor</u>	<u>Counter Number</u>	<u>Factor</u>
1	0.906	9	1.029
2	1.086	10	1.048
3	0.931	11	1.066
4	0.938	12	1.034
5	0.948	13	1.096
6	0.974	14	1.095
7	0.990	15	1.093
8	1.	16	1.094*

*Data from Counter 16 were unreliable and was therefore ignored.

[†]The counter correction factors, f_i were measured by scattering ^3He from a thick tantalum target and counting the number of scattered ^3He (per unit beam charge) with each counter and comparing this to the number of ^3He (per unit beam charge) counted by counter 8 when the magnet current was adjusted so particles of the same rigidity fell on Counter 8.

The factors f_i are given by

$$f_i = \frac{n_8(r_j)}{n_i(r_j)}$$

where $n_i(r_j)$ is the number of ^3He counted by counter i when the magnet current was adjusted so particles of rigidity r_j fell on counter i (Cocke 1964).

Table 10

Charge-State Ratios A_{ij} (See Pg. 25.)

$$E_{9\text{Be}} = 2.52 \text{ MeV}$$

i \ j	++	+++	++++
++	1	0.505 ± 0.019	2.26 ± 0.09
+++	1.857 ± 0.066	1	3.77 ± 0.07
++++	0.439 ± 0.039	0.230 ± 0.001	1

$$E_{9\text{Be}} = 1.78 \text{ MeV}$$

i \ j	+	++	+++	++++
+	1	0.091 ± 0.003	0.104 ± 0.004	0.38 ± 0.04
++	9.50 ± 0.49	1	1.094 ± 0.024	5.52 ± 0.45
+++	8.75 ± 0.50	0.899 ± 0.023	1	6.39 ± 0.45
++++	1.77 ± 0.98	0.149 ± 0.016	0.137 ± 0.004	1

Table 11

Calculated Particle Decay Widths (See Page 31.)

$${}^5\text{He} + \alpha \text{ Decay}$$

Calculation	R (${}^4\text{He} + n$) (f)	$\Gamma({}^5\text{He} + \alpha)$ (ev)
P He	2.9	158
A He	2.0	68
A He	3.0	89
A He	3.7	98
A He	4.0	111
A He	5.0	135
Alpha	2.3	210

$${}^8\text{Be} (2^+) + n \text{ Decay}$$

Calculation	R ($\alpha + \alpha$) (f)	$\Gamma({}^8\text{Be}(2^+) + n)$ (ev)
P Be	5.0	24
A Be	4.2	14
A Be	4.6	18
A Be	5.0	24
A Be	5.4	30
A Be	5.8	39
Alpha	(5.0)	7

Calculation	E_r (MeV)	$\Gamma(E_r)$ MeV
P He	0.97	1.81
A He	0.96	0.58
P Be	3.0	1.45
A Be	3.0	1.45

P He: Data from $\alpha + p$ $P_{3/2}$ phase shifts adjusted to fit ${}^4\text{He} + n$ cross-section (Dodder 1952).

A He: Data from average of measurements on ${}^5\text{He}$ ground state (Lauritsen 1965).

P Be: Data from α - α d-wave phase shift analysis (Russell 1956).

A Be: Data from average of measurements on ${}^8\text{Be}(2^+)$ (Lauritsen 1965).

Alpha: Alpha model calculation (Henley 1960).

Figure 1

Experimental arrangement. Recoil ^9Be ions at 90° were analyzed in momentum and detected with a surface-barrier counter. Alpha particles were detected with a surface-barrier counter in the target chamber. The alpha pulses were delayed by the time required for the ^9Be ions to travel through the magnet. Whenever a pulse from the ^9Be counter was in coincidence with the delayed alpha pulse, the pulses were stored on a two-dimensional pulse-height analyzer. The boxes marked 417A are single-stage preamps using a type 417A triode, the boxes marked hp A are Hewlett-Packard Type 460A wide band amplifiers, and the boxes hp B are Hewlett-Packard type 460B wide band amplifiers. (See Pg. 3.)

PLAN OF EXPERIMENT

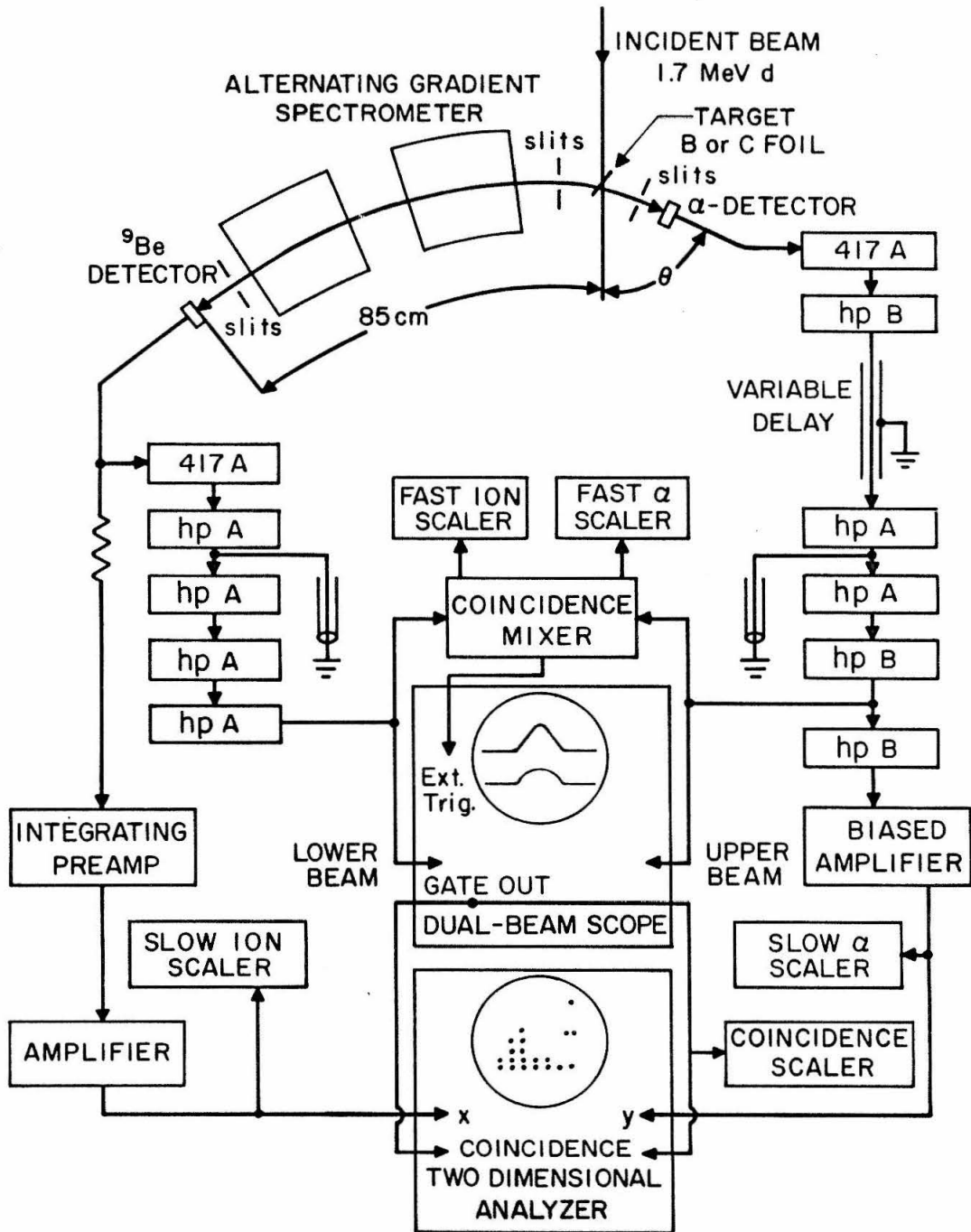


Figure 1

Figure 2

Non-coincident energy spectrum at the magnetic-spectrometer focus. The magnet current was set to admit particles with $EM/Z^2 = 4.46$ MeV. The channel number is a linear function of E , so particles with various values of M/Z^2 are separated. The positions where peaks for ${}^9\text{Be}$ and ${}^{11}\text{B}$ recoils would appear with a longer run are indicated. (See Pgs. 5 and 7.)

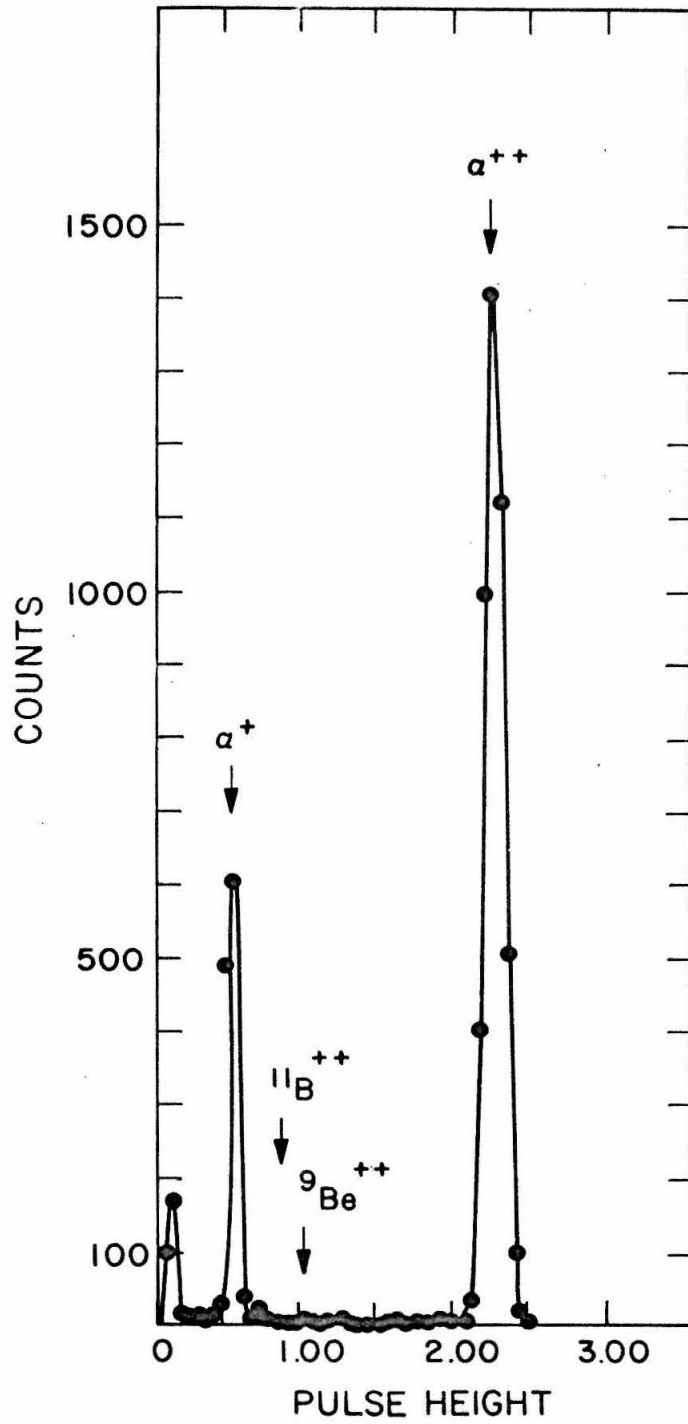
Figure 2

Figure 3

Chamber counter spectrum with slow electronics. The positions of peaks for various reactions are indicated. Also the position of the peak from protons that penetrate the depletion layer is shown. There can be no peaks from protons above the depletion layer peak. (See Pg. 6.)

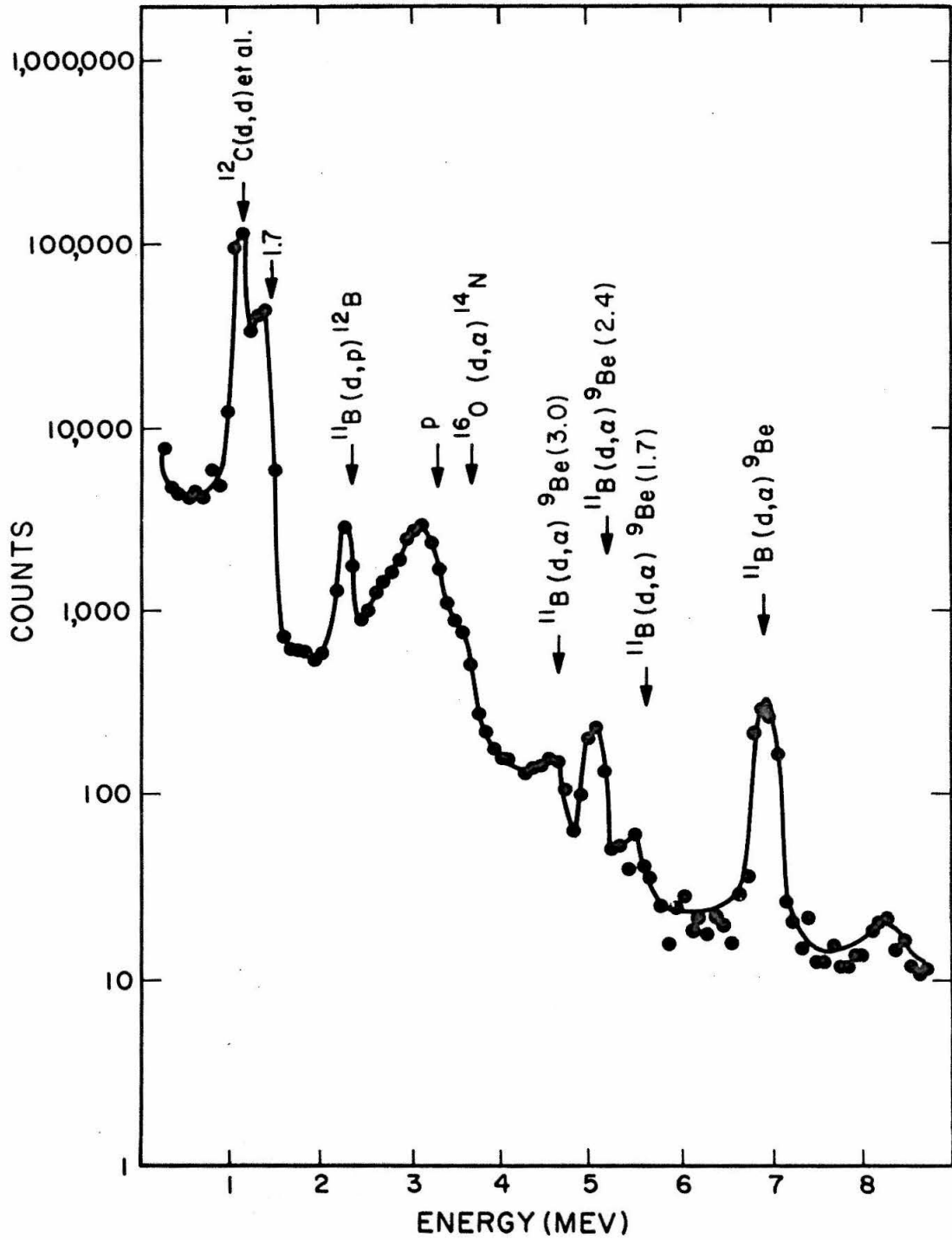


Figure 3

Figure 4

Non-coincident alpha spectrum. This spectrum was taken at a laboratory angle of 66.4° and a bombarding energy of 1.70 MeV. The spectrum is taken through the fast electronics with biased amplifier (See Figure 1) set to reject pulses below 2 MeV. The lower curve shows the result of subtracting out the α_2 peak. (See Pgs. 6 and 14.)

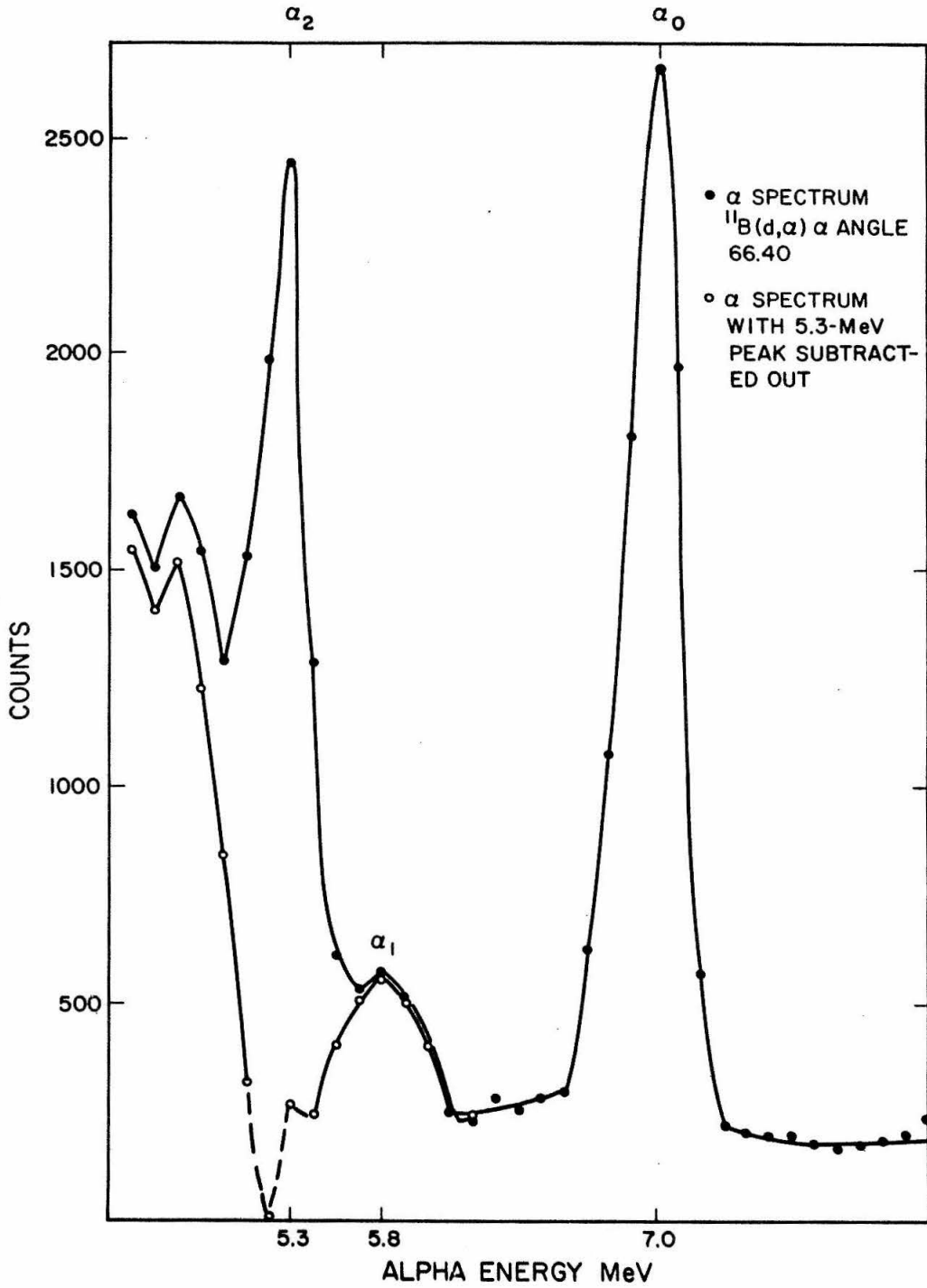
Figure 4

Figure 5

A plot of the two-dimensional analyzer output for a ${}^9\text{Be}^{++} - \alpha_2$ run on Target number 1. The magnet was set so that only ions with $EM/Z^2 = 4.46$ MeV could reach the ion counter. The height of each stick is proportional to the number of counts. The ion energy and alpha energy are determined by the position of the stick. A black rectangle marks the position of ${}^9\text{Be}^{++}$ (1.98 MeV) - α_2 (5.3 MeV) coincidences. The total charge for this run was about $800\mu\text{C}$. See Figure 5A for the analyzer output in numerical form. (See Page 8.)

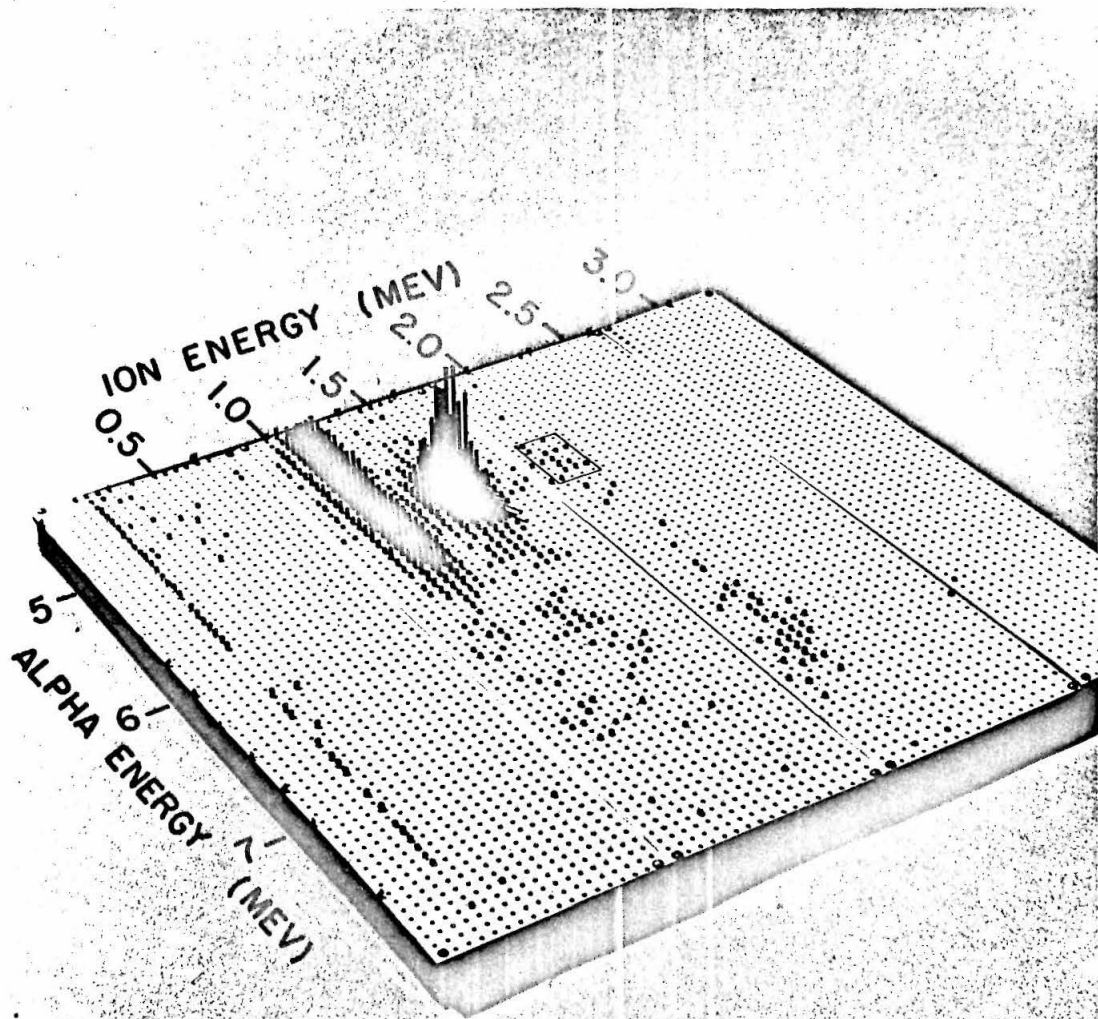


Figure 5

Figure 5A

The data of Figure 5 are shown in numerical form. (See Fig. 5.)

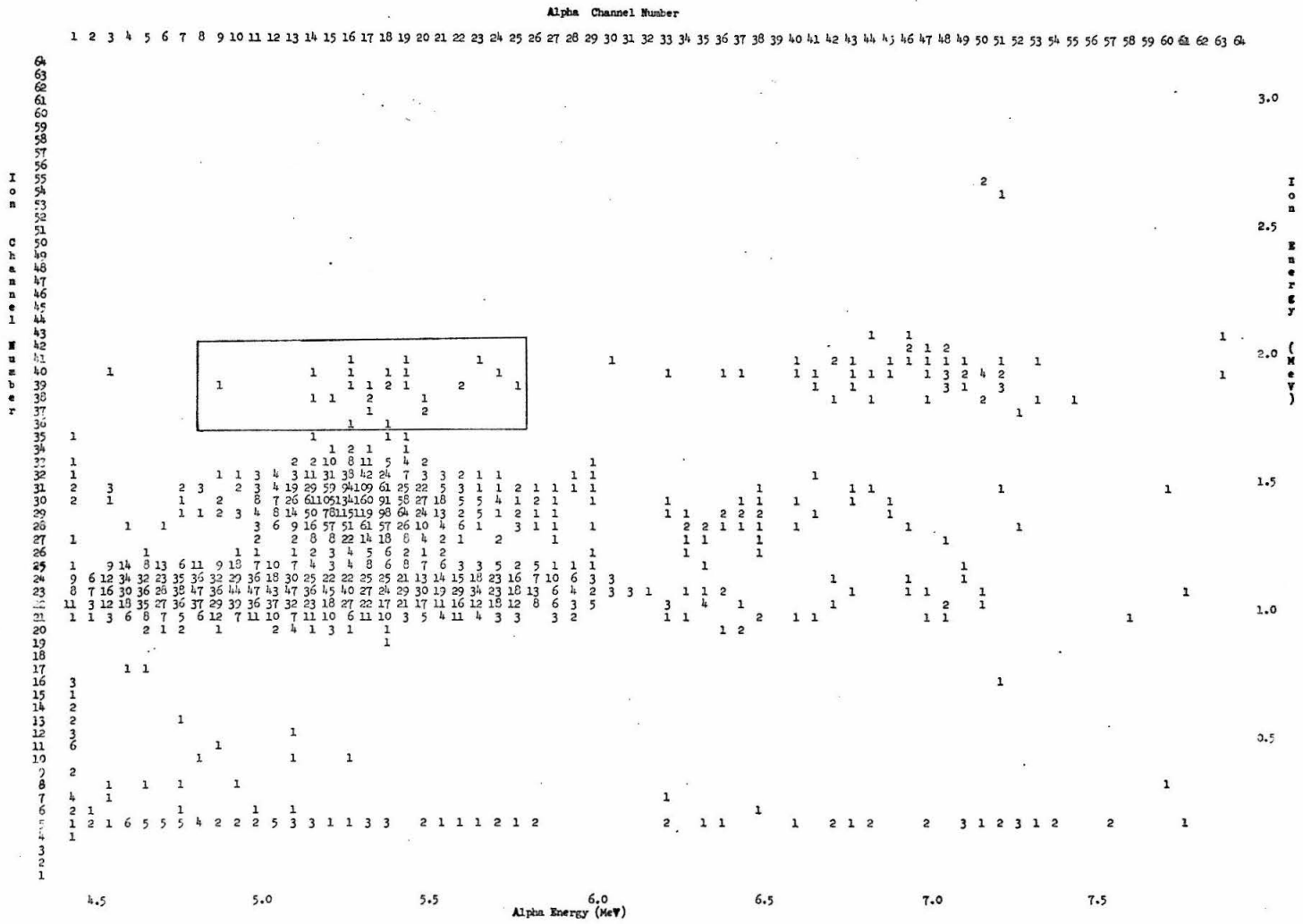


Figure 5A

Figure 6

A plot of the two-dimensional analyzer output summed over five runs (34,040 μ C of beam) of ${}^9\text{Be}^{++} - \alpha_1$ on Target number 5. The magnet was set so that only ions with $EM/Z^2 = 4.93$ MeV could reach the ion counter. A black rectangle marks the expected position of ${}^9\text{Be}^{++}$ (2.19 MeV) - α_1 (5.7 MeV) coincidences. Note that the scale and angle of view differ from those of Figure 5. See Figure 6A for the analyzer output in numerical form. (See Page 8.)

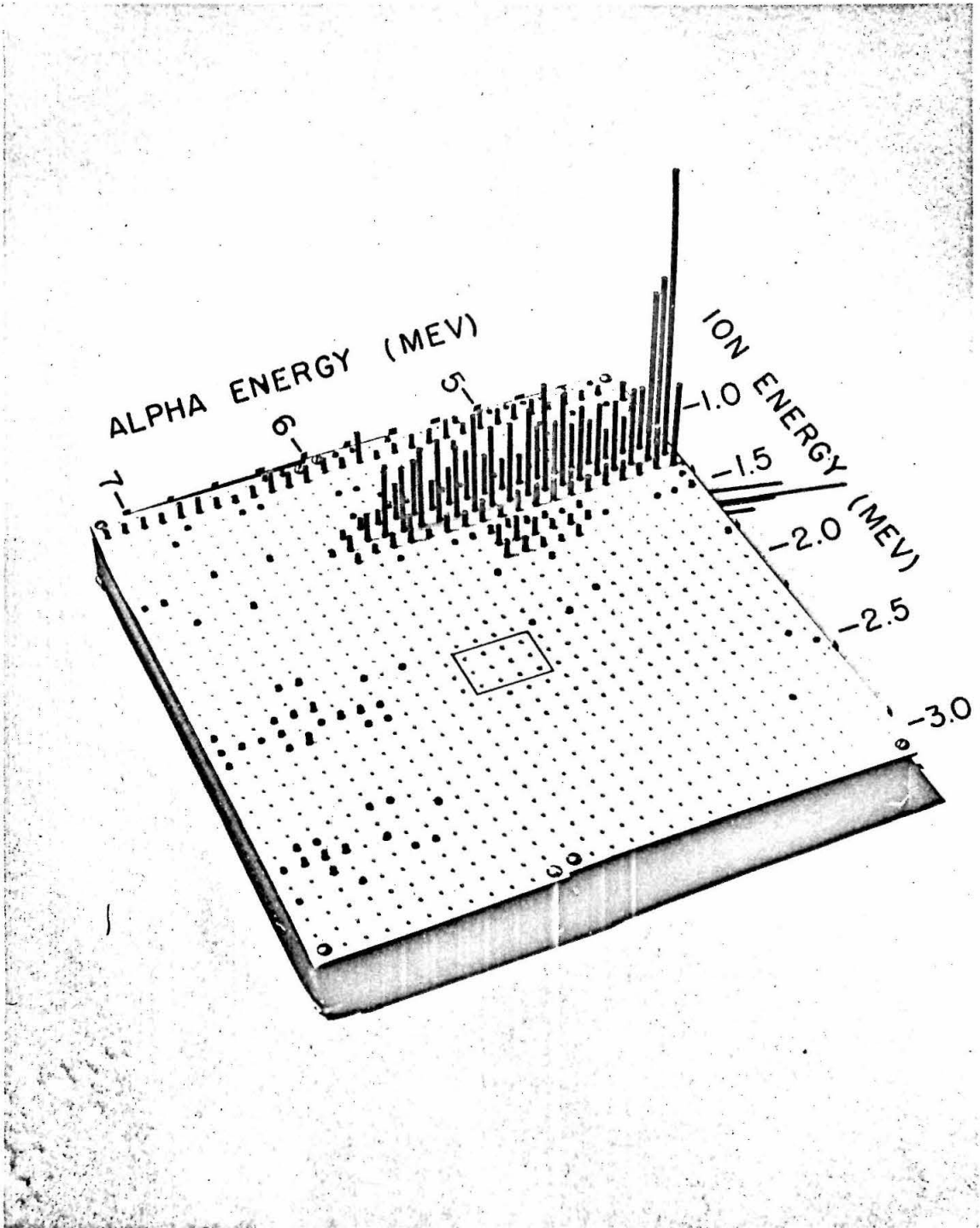


Figure 6

Figure 6A

The data of Figure 6 are shown in numerical form. (See Fig. 6.)

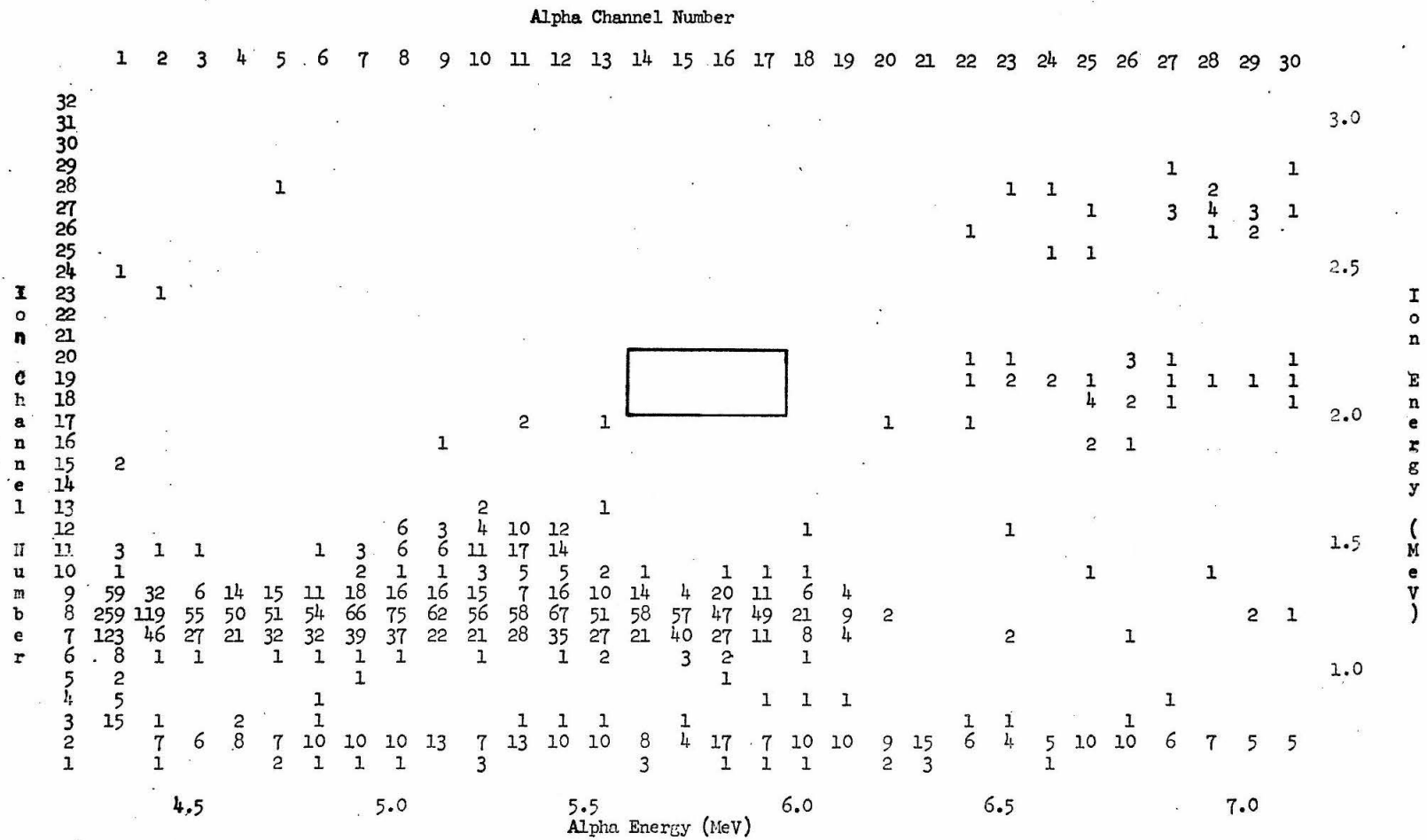


Figure 6A

Figure 7

Spectrum of ions in coincidence with 5.3 MeV alpha particles plotted against ion energy. The coincidences within the α_2 peak have been summed and plotted against ion energy. The magnet was set for $EM/Z^2 = 4.46$ MeV. (See Pg. 9.)

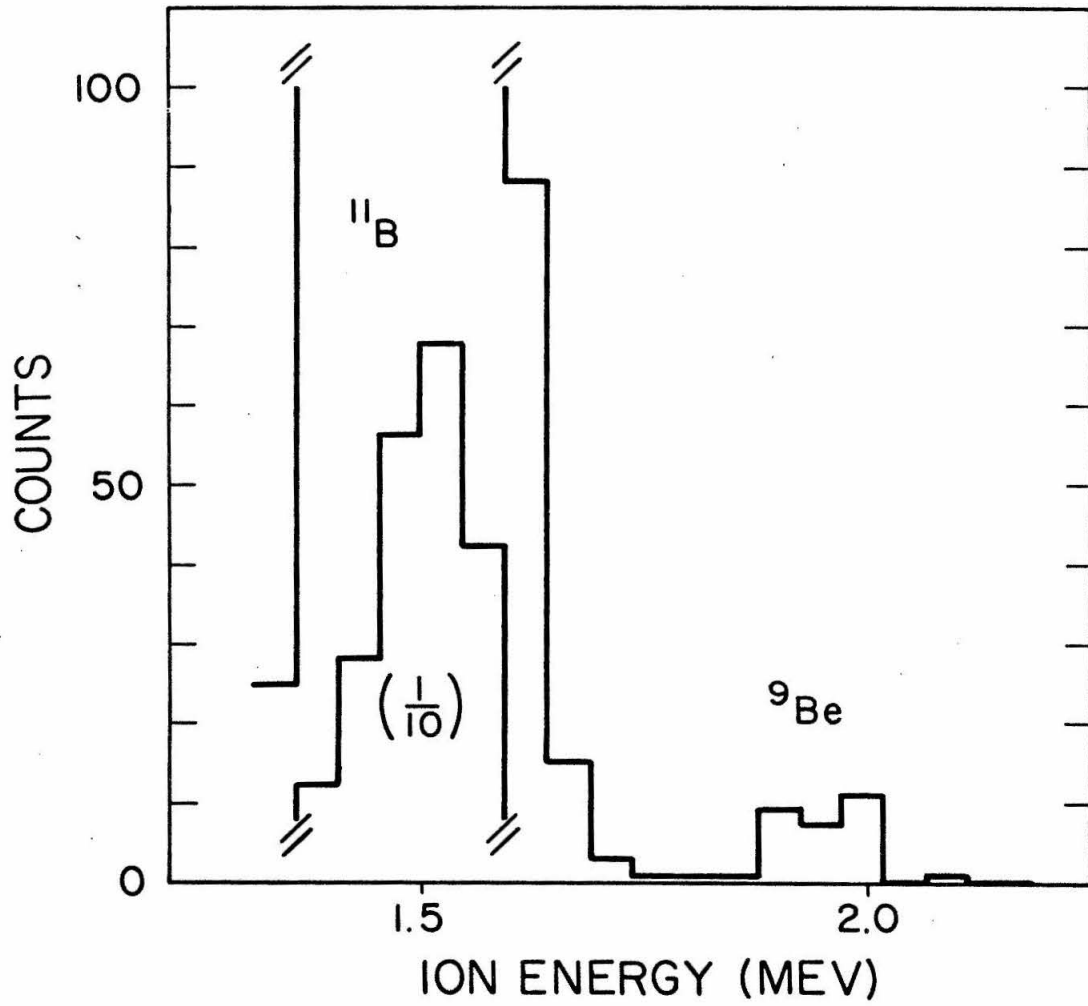


Figure 7

Figure 8

Spectrum of alpha particles in coincidence with 1.98-MeV ^9Be ions plotted against alpha energy. The coincidences within the ^9Be peak from seven runs (21,540 μC of beam) on Target 4 have been summed and plotted against alpha energy. The magnet was set for $EM/Z^2 = 4.46 \text{ MeV}$. (See Page 9.)

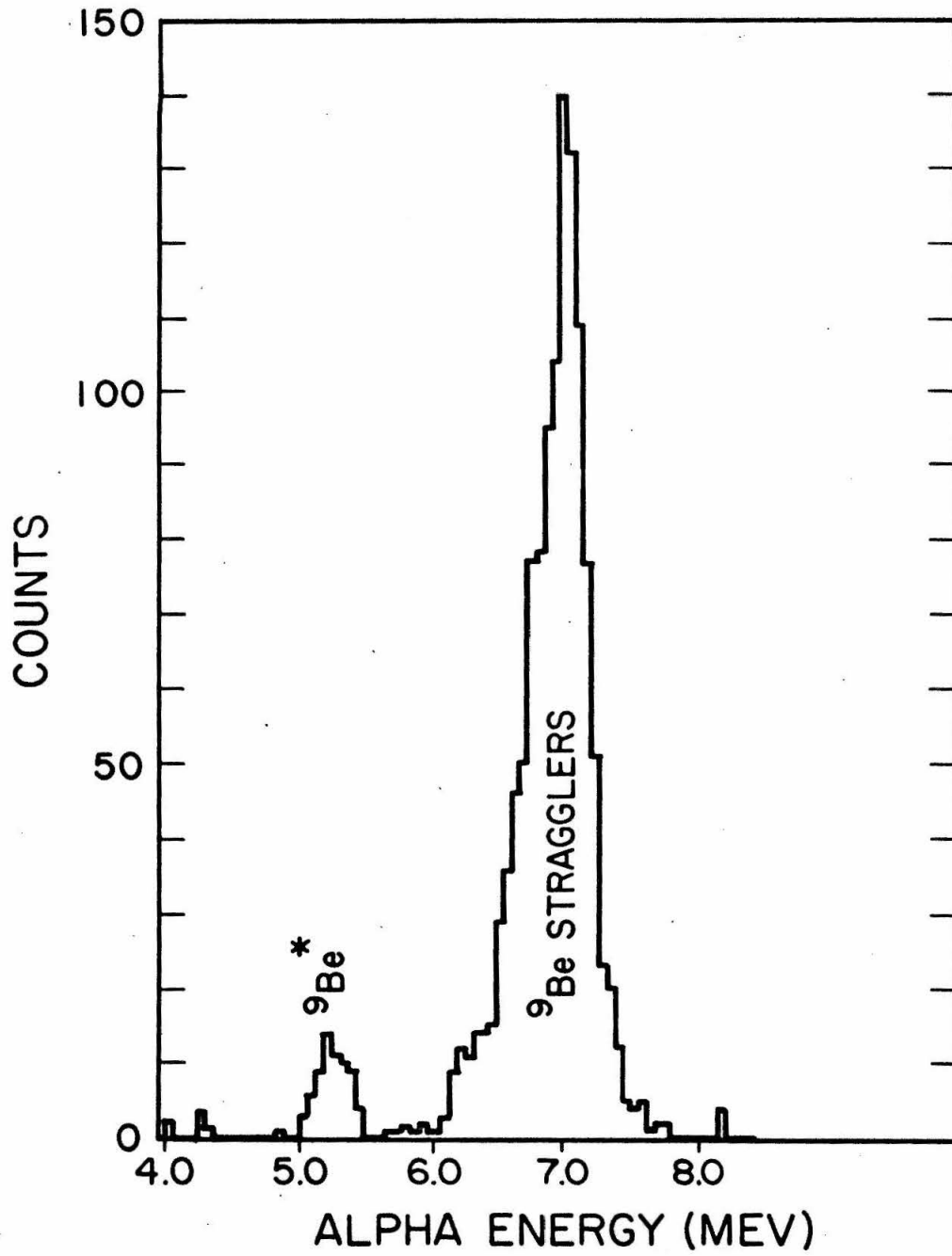


Figure 8

Figure 9

The number of alpha particles in coincidence with ions of energy of 2.19 MeV, taken in six runs (19140 μ C of beam) on Target 4, summed and plotted against alpha energy. The magnet was set for $EM/Z^2 = 4.93$ MeV. The target (No. 4) was moderately thick so that most of the counts in the region marked ${}^9\text{Be}^*$ came from the tail of the ${}^9\text{Be}$ straggler group. About one count from the 1.7-MeV level in ${}^9\text{Be}$ should have come in the region marked ${}^9\text{Be}^*$. This run, therefore, provides a measure of the number of counts from stragglers (compare with Fig. 8). (See Page 9.)

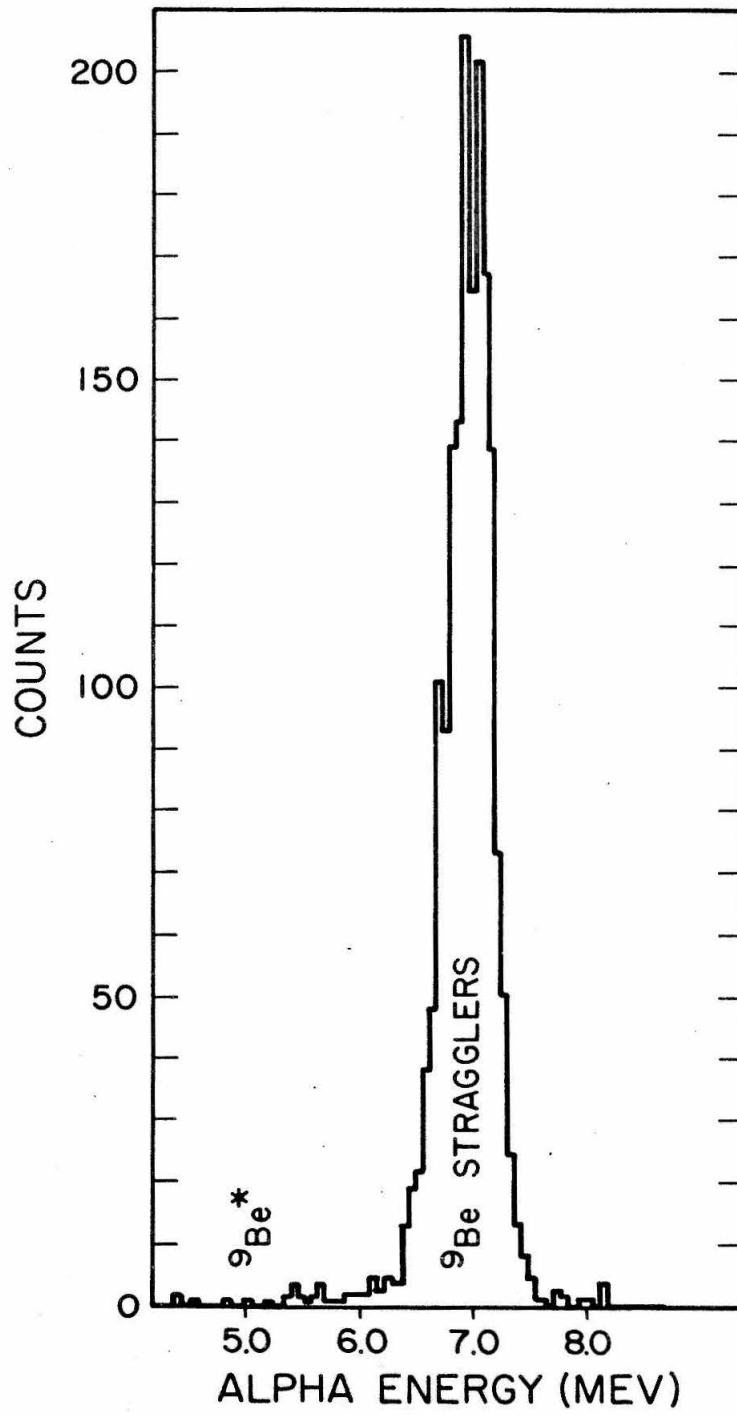


Figure 9

Figure 10

The momentum spectrum of elastically scattered protons of 1-MeV incident energy, as measured with a 25.7 cm magnetic spectrometer at a laboratory angle of 150° is shown. The target has 1.3×10^{18} at/cm² of boron. The atomic percent of other materials in the target is shown over their peaks. The lines at the top of the figure show where the front edge of the peaks for various elements should occur (See Pgs. 3 and 21.)

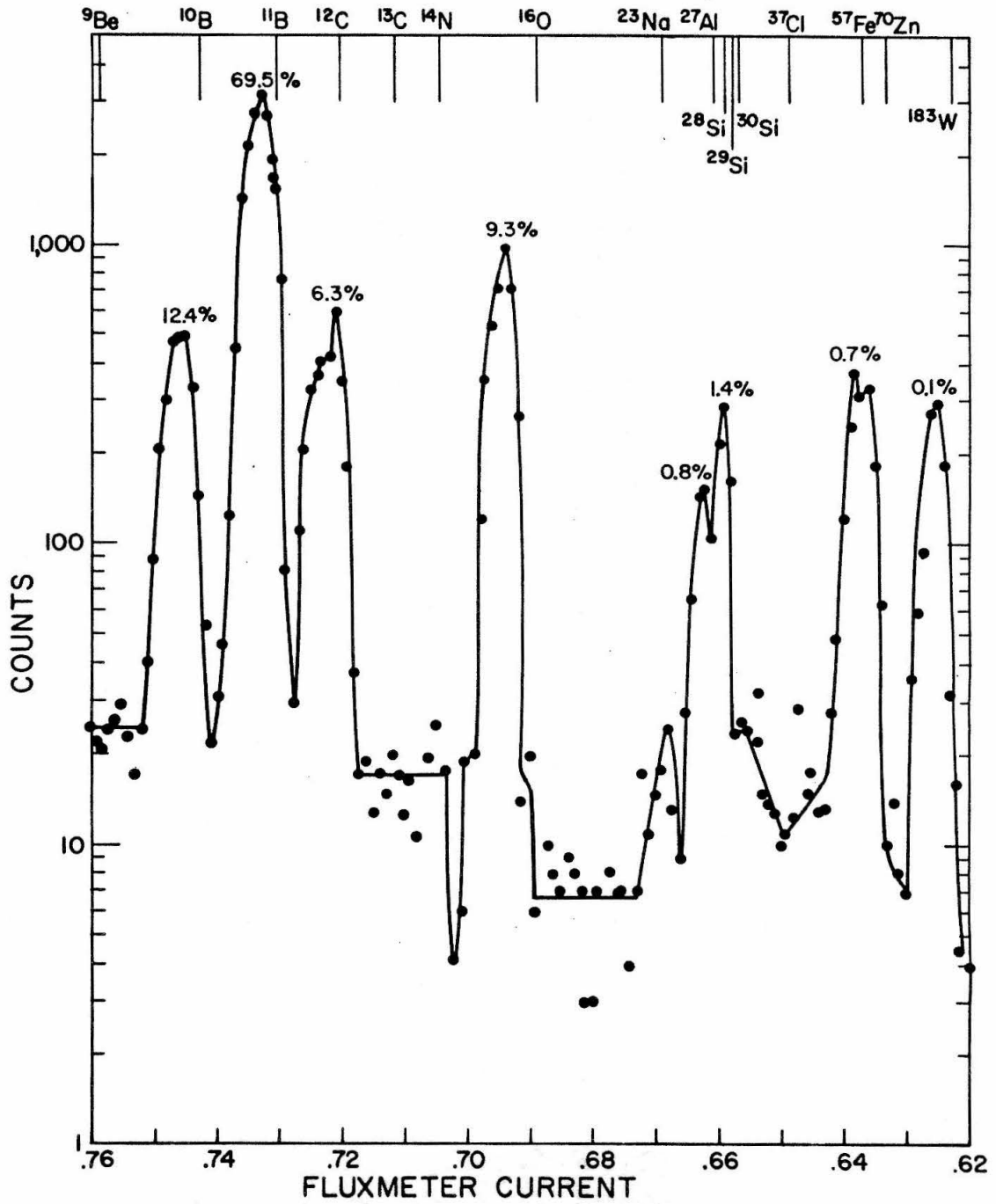


Figure 10

Figure 11

The charge-state data for 2.5-MeV ^9Be ions. The graph shows the number of counts (corrected by the counter correction factors in Table 9) for each observed charge state (2+, 3+, and 4+) plotted against the ^9Be ion energy measured by the magnetic spectrometer. (See Page 24.)

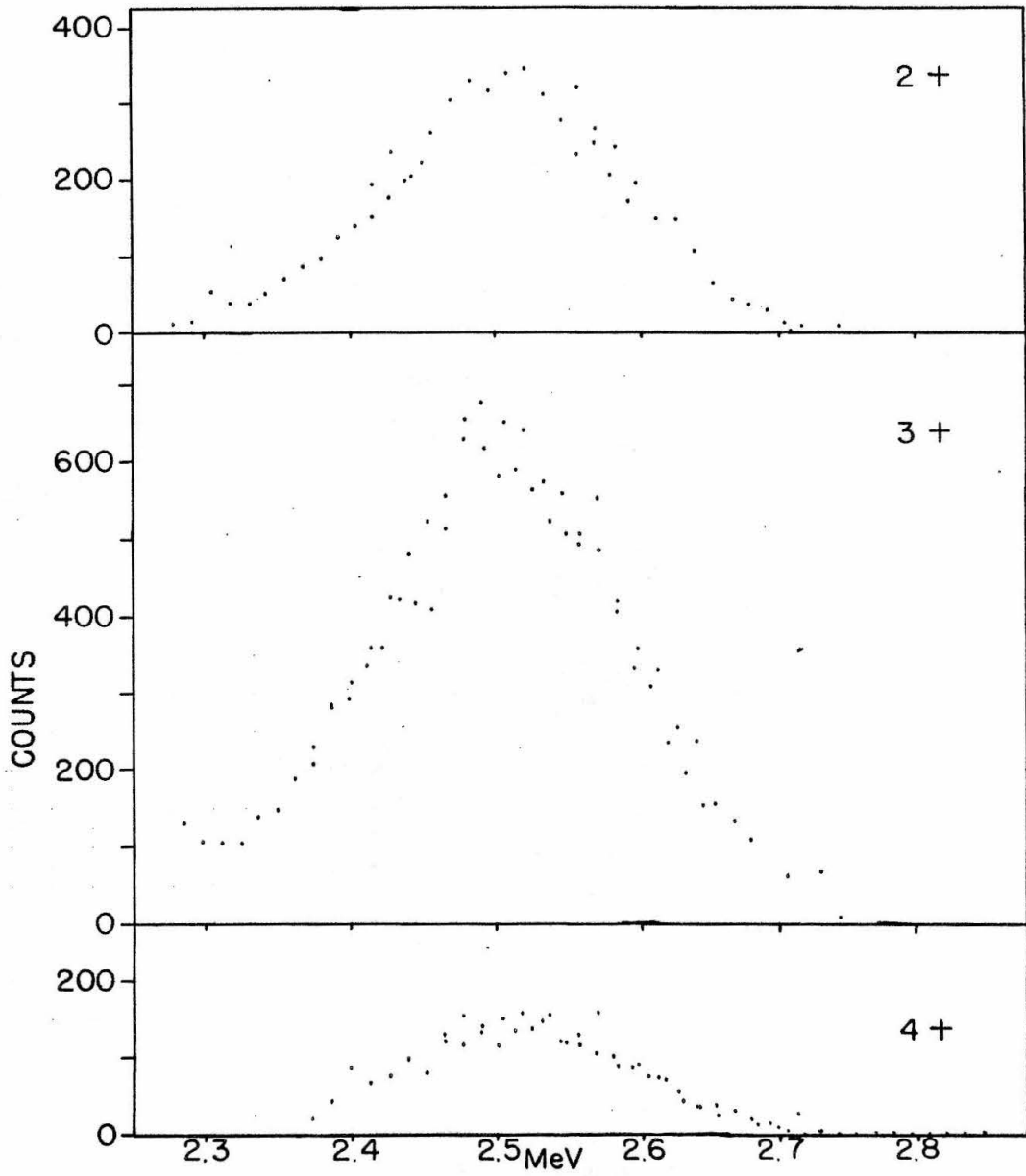


Figure 11

Figure 12

The charge-state data for 1.7-MeV ^9Be ions. The graph shows the number of counts (corrected by the counter correction factors in Table 9) for each observed charge state (1+, 2+, 3+ and 4+) plotted against the ^9Be ion energy measured by the magnetic spectrometer. (See Page 24.)

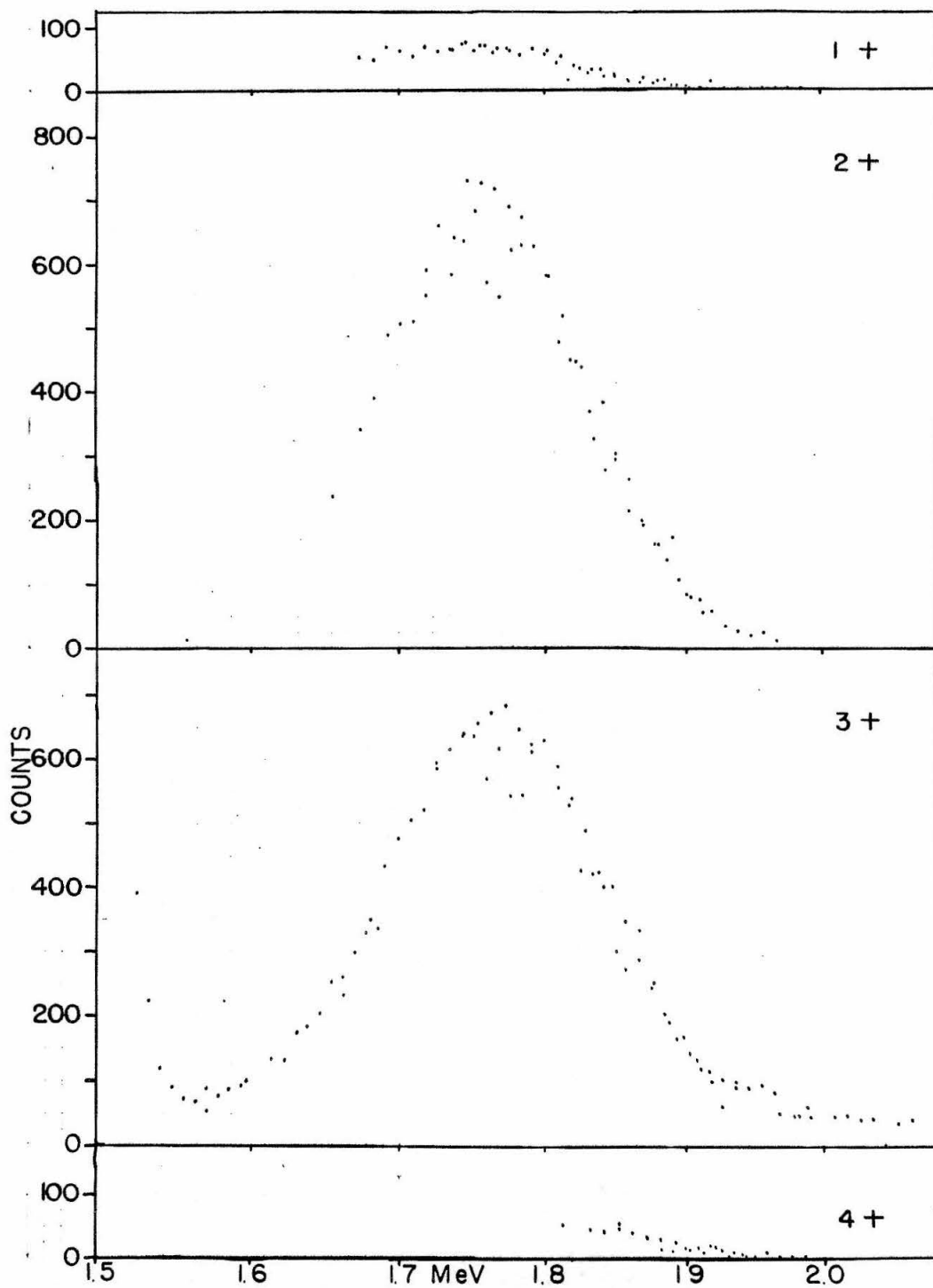


Figure 12